Cross-correlation analysis and information content of observed heads during pumping in unconfined aquifers

Deqiang Mao,[1,2] Tian-Chyi J. Yeh,[2,3] Li Wan,[1] Cheng-Haw Lee,[3] Kuo-Chin Hsu,[3] Jet-Chau Wen,[4] and Wenxi Lu[5]

Received 14 April 2012; revised 4 December 2012; accepted 17 December 2012; published 4 February 2013.

[1] Using a first-order cross-correlation analysis, this paper investigates the relationship between observed heads and hydraulic properties in the saturated and vadose zones at different times and locations of three-dimensional unconfined aquifers during pumping tests. Cross-correlation analysis is a weighted sensitivity analysis casted into a stochastic framework. It determines the relative impact of each parameter with respect to others in time and space on the observed heads according to uncertainty or spatial variability of each parameter. It reveals the information content in measured drawdowns about heterogeneity during a pumping test in an unconfined aquifer, which is critical for aquifer parameter estimation. Based on a synthetic, numerical example, our cross-correlation analysis reveals that heads in the saturated zone at late times carry the greatest nonsymmetrically weighted information content about the hydraulic conductivity (K_S) distribution within the cone of depression. On the other hand, heads in the saturated zone at early times contain the most information about the specific storage (S_S) heterogeneity in a narrow region between the observation and pumping locations. During intermediate and late times, heads in the saturated zone largely reflect the effects of saturated water content (θ_S) and pore-size parameter (α) in the thin unsaturated region near the water table above the pumping and observation locations. At last, heads in the vadose zone at late times carry the greatest information about θ_S and α around the observation point.

Citation: Mao, D., T.-C. J. Yeh, L. Wan, C.-H. Lee, K.-C. Hsu, J.-C. Wen, and W. Lu (2013), Cross-correlation analysis and information content of observed heads during pumping in unconfined aquifers, *Water Resour. Res.*, *49*, doi:10.1002/wrcr.20066.

1. Introduction

[2] Analysis of pumping tests in unconfined aquifers has been an active research topic for the last few decades. For example, *Boulton* [1954], *Neuman* [1972], *Moench* [1997], *Mathias and Butler* [2006], *Moench* [2008], and *Mishra and Neuman* [2010] developed analytical models for estimating parameters for homogeneous aquifers, whereas *Zhu and Yeh* [2008], *Zhu et al*. [2011], and *Cardiff and Barrash* [2011] developed numerical inverse models to estimate spatially distributed aquifer parameters. *Nwankwor et al*. [1992], *Akindunni and Gillham* [1992], *Narasimhan and Zhu* [1993], and *Mao et al*. [2011] investigated the causes of the unique S-shaped drawdown-time curve observed during pumping tests in unconfined aquifers. Few studies have examined the information content of measured drawdowns about heterogeneity in the saturated and vadose zones during a pumping test in an unconfined aquifer. Similarly, few have attempted to explain the implications of measured drawdowns on the spatial distributions of estimated parameters from pumping tests.

[3] Methods for analyzing pumping tests in confined aquifers have been well established in comparison with those in unconfined aquifers. Similarly, over the past decades, numerous studies based on the deterministic and stochastic approaches have investigated the effects of heterogeneity and its impacts on pumping test analysis. For example, *Barker and Herbert* [1982], *Hunt* [1985], *McElwee* [1987], *Butler* [1988, 1990], *Streltsova* [1988], *Butler and McElwee* [1990], and *Butler and Liu* [1991, 1993] defined distinct patterns of heterogeneity using simplified aquifer geometries with singular discontinuities to investigate their effects on the drawdown. Others such as *Oliver* [1993] and *Leven and Dietrich* [2006] used Frechet derivative and sensitivity, respectively, to investigate the influence of transmissivity and storativity on drawdowns during pumping tests.

[1]School of Water Resources and Environmental Science, China University of Geosciences, Beijing, China.
[2]Department of Hydrology and Water Resources, The University of Arizona, Tucson, Arizona, USA.
[3]Department of Resources Engineering, National Cheng Kung University, Tainan, Taiwan.
[4]Department of Safety, Health and Environmental Engineering, Research Center for Soil and Water Resources and Natural Disaster Prevention, National Yunlin University of Science and Technology, Touliu, Yunlin, Taiwan.
[5]College of Environment and Resources, Jilin University, Changchun, Jilin, China.

Corresponding author: D. Mao, Department of Hydrology and Water Resources, The University of Arizona, Tucson, AZ 85721, USA. (deqiang@email.arizona.edu)

0043-1397/13/10.1002/wrcr.20066

[4] *Naff* [1991], *Neuman and Orr* [1993], *Desbarats* [1992, 1993], *Indelman and Dagan* [1993a, 1993b], *Sánchez-Vila et al*. [1995], *Tiedeman et al*. [1995], *Tartakovsky and Neuman* [1998], *Indelman* [2003], and others investigated the relationship between the statistics describing spatial variability of small-scale parameters of aquifers and the effective parameters of equivalent homogeneous aquifers. Others employed the cross correlation between observed heads and spatial heterogeneity of hydraulic properties to estimate spatial distributed hydraulic parameters in confined aquifers [e.g., *Dagan*, 1982; *Kitanidis and Vomvoris*, 1983; *Hoeksema and Kitanidis*, 1984; *Kitanidis*, 1995; *Yeh et al*., 1995, 1996] as well as to conduct hydraulic tomography (HT) analysis [e.g., *Yeh and Liu*, 2000; *Zhu and Yeh*, 2005; *Illman et al*., 2009; *Xiang et al*., 2009; *Berg and Illman*, 2011].

[5] Recently, *Wu et al*. [2005] used the cross-correlation analysis to investigate the meanings of and problems associated with the transmissivity (T) and storativity (S) estimates from Theis analysis. *Huang et al*. [2011] used the cross correlation to elucidate pumping location dependence nature of T and S estimates based on a single pumping test data using either homogeneous or heterogeneous conceptual aquifer model, and to explain the robustness of joint interpretation of sequential pumping tests for mapping aquifer heterogeneity. More recently, Sun et al. (A temporal sampling strategy for transient hydraulic tomography analysis, submitted to *Water Resources Research*, 2012) conducted the cross-correlation analysis to investigate temporal and spatial sampling strategies of hydraulic tomography in two-dimensional (2-D) depth-averaged aquifers.

[6] Although no study has conducted sensitivity or cross-correlation analysis of the flow during pumping tests in unconfined aquifer, cross-correlation analysis has been developed for estimating hydraulic parameters of variably saturated heterogeneous media during infiltration [*Yeh and Zhang*, 1996; *Zhang and Yeh*, 1997; *Li and Yeh*, 1998, 1999; *Hughson and Yeh*, 2000]. *Mao et al*. [2011] recently used it to investigate the effects of heterogeneity on uncertainty in predicted drawdown-time curves. None of these studies have provided insights to the relationship between the observed head and aquifer parameter distributions.

[7] The objective of this paper therefore is to explore the cross correlation between observed heads and hydraulic parameters of saturated and vadose zones during pumping tests in unconfined aquifers. Based on the results of the cross-correlation analysis in a synthetic unconfined aquifer, this paper discusses the information content embedded in the observed head at different time periods of the pumping test about different parameters. Furthermore, it examines the inference about the spatial distribution of parameters from the observed drawdown at the different time periods.

2. Methodology

2.1. Equation for Variably Saturated Groundwater Flow

[8] This study assumes that flow in unconfined aquifers can be adequately described by the governing equation for flow through heterogeneous variably saturated geological media [see *Mao et al*., 2011]. That is,

$$\begin{aligned}\nabla\cdot[K(h,\mathbf{x})\nabla(h+z)]+Q(\mathbf{x}_\mathrm{p})&=\omega S_s(\mathbf{x})\frac{\partial h}{\partial t}+\frac{\partial\theta}{\partial t}\\&=[\omega S_s(\mathbf{x})+C(h,\mathbf{x})]\frac{\partial h}{\partial t},\end{aligned}\tag{1}$$

subject to boundary and initial conditions:

$$\begin{aligned}&h|_{\Gamma_1}=h_1, K(h,\mathbf{x})\nabla(h+z)\cdot\mathbf{n}|_{\Gamma_2}=q, h|_{t=0}=h_0,\\&\Gamma=\Gamma_1\cup\Gamma_2,\end{aligned}\tag{2}$$

where ∇ is the differential operator, t is the time, θ represents the volumetric moisture content, and z is the elevation (positive upward), h is the pressure head and is positive when the medium is saturated and negative when unsaturated. $Q(\mathbf{x}_p)$ is the pumping rate per unit volume of the aquifer at location $\mathbf{x}_p$. The saturation index ω is equal to 1 if the medium is saturated and 0 if the medium is unsaturated. The term $S_S(\mathbf{x})$ represents the specific storage, $C(h,\mathbf{x})$ is the soil moisture capacity, and $K(h,\mathbf{x})$ is the hydraulic conductivity constitutive function at location $\mathbf{x}$. In equation (2), h_1 is the prescribed head at Γ_1, $\mathbf{n}$ is the normal vector to the boundary Γ_2, q is the specific flux at Γ_2, and h_0 is the initial pressure head.

[9] We adopt *Gardner-Russo* model [*Russo*, 1988] to describe the hydraulic conductivity-pressure head relationship and the corresponding consistent moisture water content and pressure head relationship. That is,

$$K(h,\mathbf{x})=K_s(\mathbf{x})e^{\alpha(\mathbf{x})h},\tag{3}$$

where K_S is the saturated conductivity, and α is the pore-size distribution parameter;

$$\theta(h)=(\theta_S-\theta_r)\left[e^{0.5\alpha h}(1-0.5\alpha h)\right]^{2/2+m}+\theta_r,\tag{4}$$

where θ_S and θ_r are the saturated and residual moisture content, respectively (both are dimensionless). The parameter m (dimensionless) is related to tortuosity of the soil and is assumed to be zero in this study. Equations (1)–(4) will be used in the following cross-correlation analysis.

2.2. Cross-Correlation Analysis

[10] Following the methodologies by *Li and Yeh* [1998, 1999] and *Hughson and Yeh* [2000], we develop cross-correlation analysis for flow to a well during a pumping test in homogeneous and heterogeneous unconfined aquifers. They are described below.

2.2.1. Homogeneous Aquifers

[11] The purpose of analyzing the cross correlation between the observed head at a given location and a given parameter of the homogeneous aquifer is to study the relative influence of each aquifer parameter on the drawdown during different pumping time periods. To do so, the natural log of each hydraulic parameter in equations (1)–(4) is conceptualized as a random variable, with a mean value plus a random perturbation. That is,

$$\begin{aligned}&\ln K_S=f=\bar f+f' \quad \ln S_S=s=\bar s+s'\\&\ln\alpha=a=\bar a+a' \quad \ln\theta_S=t_s=\bar t_s+t'_S,\end{aligned}$$

where the overbar denotes the mean and the prime for the perturbation. The perturbations, f', s', a', and t'_S have the variances, σ_f^2, σ_s^2, σ_a^2, and σ_{tS}^2, respectively. The conceptualization of each parameter as a random variable in the homogeneous case aims to represent the uncertainty associated with the parameter value because of no measurement or measurement errors of this parameter instead of spatial variability of the parameter.

[12] Likewise, the system response (i.e., pressure head) is represented as a random variable as a result of the uncertainty in the parameters, which can be expressed in terms of a mean and a perturbation. Specifically, the head can first be expanded in the Taylor series about the mean values of the parameters. Then, by neglecting the second-order and higher-order terms in the series, we have the first-order approximation for the pressure head:

$$h(\mathbf{x},t)=\bar{h}(\mathbf{x},t)+h'(\mathbf{x},t)\approx\bar{h}(\mathbf{x},t)+f'\left.\frac{\partial h(\mathbf{x},t)}{\partial f}\right|_{\overline{P}} +s'\left.\frac{\partial h(\mathbf{x},t)}{\partial s}\right|_{\overline{P}}+a'\left.\frac{\partial h(\mathbf{x},t)}{\partial a}\right|_{\overline{P}}+t'_S\left.\frac{\partial h(\mathbf{x},t)}{\partial t_S}\right|_{\overline{P}}, \quad (5)$$

where the derivative is the Jacobian, the sensitivity of $h(\mathbf{x}, t)$ to the change of a given parameter. The vertical bar with subscript $\overline{P}$ implies that the sensitivity is evaluated at the mean values of all parameters. After subtracting the mean part from both sides of the equation (5), the head perturbation is

$$h'(\mathbf{x},t)=f'J_{hf}(\mathbf{x},t)+s'J_{hs}(\mathbf{x},t)+a'J_{ha}(\mathbf{x},t)+t'_SJ_{ht_S}(\mathbf{x},t) \quad (6)$$

in which J is the Jacobian.

[13] Assuming that the perturbations of all the hydraulic parameters are mutually independent, multiplying equation (6) by itself on both sides and taking the expected value of the product, we have

$$\sigma_h^2(\mathbf{x},t)=\left(J_{hf}(\mathbf{x},t)\right)^2\sigma_f^2+(J_{hs}(\mathbf{x},t))^2\sigma_s^2+(J_{ha}(\mathbf{x},t))^2\sigma_a^2 +(J_{hts}(\mathbf{x},t))^2\sigma_{t_S}^2. \quad (7)$$

[14] In equation (7), $\sigma_h^2(\mathbf{x},t)$ is the head variance at $(\mathbf{x},t)$, representing possible deviation of the observed head from the mean head at a given $(\mathbf{x},t)$, which is determined with the mean values of the parameters.

[15] Based on equation (6), the cross-covariance between heads and a parameter can be derived by multiplying the parameter perturbation on both sides of the equation and taking the expected value of the resultant equation. That is,

$$\begin{array}{ll}\sigma_{hf}^2(\mathbf{x},t)=J_{hf}(\mathbf{x},t)\sigma_f^2 & \sigma_{hs}^2(\mathbf{x},t)=J_{hs}(\mathbf{x},t)\sigma_s^2\\ \sigma_{ha}^2(\mathbf{x},t)=J_{ha}(\mathbf{x},t)\sigma_a^2 & \sigma_{ht_S}^2(\mathbf{x},t)=J_{ht_S}(\mathbf{x},t)\sigma_{t_S}^2,\end{array} \quad (8)$$

where $\sigma_{hf}^2(\mathbf{x},t)$ is the cross-covariances between the head and $\ln K_S$; $\sigma_{hs}^2(\mathbf{x},t)$ is the cross-covariances between the head and $\ln S_S$; $\sigma_{ha}^2(\mathbf{x},t)$ is the cross-covariances between the head and $\ln\alpha$; $\sigma_{ht_s}^2(\mathbf{x},t)$ is the cross-covariances between the head and $\ln\theta_s$. These cross-covariances can be normalized by the square root of head variance and the corresponding parameter variance to derive their cross-correlation functions. For example, the cross correlation between the head at $(\mathbf{x},t)$ and the hydraulic conductivity perturbation is

$$\rho_{hf}(\mathbf{x},t)=\frac{J_{hf}(\mathbf{x},t)\sigma_f{}^2}{\sqrt{\sigma_h^2(\mathbf{x},t)\sigma_f^2}}=\frac{J_{hf}(\mathbf{x},t)\sigma_f}{\sigma_h(\mathbf{x},t)}. \quad (9)$$

[16] The cross correlation is different from the sensitivity. The sensitivity depicts the change in head per unit change of a given parameter value without considering the influence of other parameters. On the other hand, the cross correlation represents the fraction of the contribution of a parameter uncertainty (standard deviation) to the head uncertainty (deviation) at a given spatial location and time. The standard deviation of head is a collective contribution from uncertainties of all parameters (equation (7)). The cross correlation thus ranges between $+1$ and -1, whereas the sensitivity could vary by a wider range. When the uncertainty of each parameter is the same, the cross correlation is merely the relative sensitivity. Under saturated steady flow conditions, the cross correlation becomes 1 regardless of the head location except at constant head boundaries. This implies that head anywhere in the aquifer is directly related to the uniform hydraulic conductivity in spite of the fact that the sensitivity is small.

2.2.2. Heterogeneous Media

[17] For the investigation of effects of spatial variability of each hydraulic parameter on the head, we assume the natural log of each parameter at every location of the aquifer as a random variable. Therefore, the heterogeneous property field of the aquifer is conceptualized as a collection of random variables: a stochastic process or a random field. Each property will have a mean value and perturbation, which represents uncertainties due to the spatial variability as well as lack of measurements. That is,

$$\begin{array}{ll}\ln K_S(\mathbf{x})=f(\mathbf{x})=\overline{f}+f'(\mathbf{x}) & \ln S_S(\mathbf{x})=s(\mathbf{x})=\bar{s}+s'(\mathbf{x})\\ \ln\alpha(\mathbf{x})=a(\mathbf{x})=\bar{a}+a'(\mathbf{x}) & \ln\theta_S(\mathbf{x})=t_s(\mathbf{x})=\bar{t}_s+t'_s(\mathbf{x}).\end{array}$$

[18] Similarly, the head perturbation around its mean can be approximated using the first-order approach as

$$h'(\mathbf{x}_i,t)\approx\left.\frac{\partial h(\mathbf{x}_i,t)}{\partial f_j}\right|_{\overline{P}}f'_j+\left.\frac{\partial h(\mathbf{x}_i,t)}{\partial s_j}\right|_{\overline{P}}s'_j+\left.\frac{\partial h(\mathbf{x}_i,t)}{\partial a_j}\right|_{\overline{P}}a'_j +\left.\frac{\partial h(\mathbf{x}_i,t)}{\partial t_{sj}}\right|_{\overline{P}}t'_{sj}. \quad (10)$$

[19] The derivatives (sensitivity) in equation (10) represent the head change at location $\mathbf{x}_i$ ($i=1,\ldots,N_h$, which is the total number of observation data) at time t due to unit change in the parameter at any location ($j=1,\ldots,N_p$, which is the total number of parameters in the aquifer, i.e., number of elements in a finite element domain). In equation (10), the Einstein's summation convention over the repeated suffix is used. In other words, the head perturbation at $(\mathbf{x}_i, t)$ is a weighted sum of parameter perturbation, f', s', a', and t'_s everywhere in the aquifer. The weights are the corresponding sensitivity values. Equation (10) can also be written in a matrix form:

$$\mathbf{h}'=\mathbf{J}_{hf}\mathbf{f}'+\mathbf{J}_{hs}\mathbf{s}'+\mathbf{J}_{ha}\mathbf{a}'+\mathbf{J}_{ht_s}\mathbf{t}'_\mathbf{s}. \quad (11)$$

[20] If there are N_h head observations, $\mathbf{h}'$ is a $N_h\times 1$ vector, $\mathbf{f}'$, $\mathbf{s}'$, $\mathbf{a}'$, and $\mathbf{t}'_\mathbf{s}$ are the $N_p\times 1$ vectors. Different $\mathbf{J}$ are the $N_h\times N_p$ Jacobian matrices. Assuming that different parameters are mutually independent of each other, the cross-covariance matrices between h at $(\mathbf{x}_i, t)$ and different given parameters everywhere in the domain become

$$\begin{array}{ll}\mathbf{R}_{hf}=\mathbf{J}_{hf}\mathbf{R}_{ff} & \mathbf{R}_{hs}=\mathbf{J}_{hs}\mathbf{R}_{ss}\\ \mathbf{R}_{ha}=\mathbf{J}_{ha}\mathbf{R}_{aa} & \mathbf{R}_{ht_s}=\mathbf{J}_{ht_s}\mathbf{R}_{t_st_s}.\end{array} \quad (12)$$

[21] $\mathbf{R}_{ff}$, $\mathbf{R}_{ss}$, $\mathbf{R}_{aa}$, and $\mathbf{R}_{t_s t_s}$ are the $N_p \times N_p$ covariance matrices describing the spatial statistics of parameter perturbations, $\mathbf{f}'$, $\mathbf{s}'$, $\mathbf{a}'$, and $\mathbf{t}'_{\mathbf{s}}$, respectively. They are modeled with an exponential function with the same correlation scales L_x, L_y, and L_z in x, y, and z directions, respectively. Physically, the correlation scales represent the average length, width, and thickness of the heterogeneity, respectively. The corresponding head covariance matrix based on equation (11) is given as

$$\mathbf{R}_{hh} = \mathbf{J}_{hf}\mathbf{R}_{ff}\mathbf{J}_{hf}^T + \mathbf{J}_{hs}\mathbf{R}_{ss}\mathbf{J}_{hs}^T + \mathbf{J}_{ha}\mathbf{R}_{aa}\mathbf{J}_{ha}^T + \mathbf{J}_{ht_s}\mathbf{R}_{t_s t_s}\mathbf{J}_{ht_s}^T. \quad (13)$$

[22] The superscript T denotes the transpose. The diagonal components of $\mathbf{R}_{hh}$ are the head variances $\sigma_h^2(\mathbf{x}_i, t)$, which represent the uncertainty in heads at $(\mathbf{x}_i, t)$.

[23] The cross-correlation matrices between head at $(\mathbf{x}_i, t)$ and different parameters can then be obtained by normalizing the cross-covariances in equation (12) with the square root of the product of the variances of h at $(\mathbf{x}_i, t)$ and the corresponding variance of the parameter. For example,

$$\boldsymbol{\rho}_{hf}(t) = \frac{\mathbf{R}_{hf}(t)}{\sqrt{\sigma_h^2(\mathbf{x}_i, t)\sigma_f^2}} = \frac{\mathbf{J}_{hf}(t)\mathbf{R}_{ff}}{\sqrt{\sigma_h^2(\mathbf{x}_i, t)\sigma_f^2}}. \quad (14)$$

[24] This cross-correlation matrix represents the fraction of the head perturbation at $(\mathbf{x}_i, t)$ $(i = 1, \ldots, N_h)$ influenced by the uncertainty of ln$K$ values at each location $\mathbf{x}_j$ $(j = 1, \ldots, N_p)$. These cross-correlation functions are evaluated with the given mean values of all parameters, boundary/initial conditions, and a pumping rate. The cross-correlation analysis is a sensitivity analysis casted in a stochastic framework. It employs the stochastic or geostatistic concept. It includes not only the variance of the parameter but also the spatial covariance function or variogram of the parameter to depict how an observed head is influenced by unknown spatial variability of parameters. Physically, the variogram represents the average dimensions of "geofabrics" (i.e., layers, stratifications, or structures) in the aquifer. The cross-correlation analysis therefore considers not only the governing flow equation and the most likely value of hydraulic properties (as in sensitivity analysis), but also the possible magnitude of heterogeneity (variance) and the geologic fabrics of an aquifer to investigate how the head at $(\mathbf{x}_i, t)$ is affected by the heterogeneity in every part of the aquifer.

2.3. Sensitivity Analysis

[25] This section develops the sensitivity of the head with respect to every parameter, which is required in the evaluation of cross correlations. Here, we employed a sensitivity equation method for the homogeneous aquifer model and an adjoint state method for the heterogeneous aquifer model for computational efficiency.

2.3.1. Sensitivity Equation Method

[26] Treating the parameters in equation (1) as homogeneous, we take the derivative of the equation with respect to a given parameter P to obtain the following expression:

$$\frac{\partial}{\partial P}\{\nabla \cdot [K(h,\mathbf{x})\nabla(h+z)]\} = \frac{\partial}{\partial P}\left\{[\omega S_s + C(h,\mathbf{x})]\frac{\partial h}{\partial t}\right\}. \quad (15)$$

[27] If we expand equation (15) and let $\phi = \partial h / \partial P$, then we have

$$\nabla \cdot [K(h,\mathbf{x})\nabla\phi] - [\omega S_s + C(h)]\frac{\partial \phi}{\partial t} = \left[\frac{dC(h)}{\partial P} + \omega\frac{\partial S_s}{\partial P}\right]\frac{\partial h}{\partial t} - \nabla \cdot \left[\frac{dK(h)}{\partial P}\nabla(h+z)\right]. \quad (16)$$

[28] The terms on the right-hand side of equation (16) are the "source/sink" terms. The derivative of moisture capacity and that of conductivity are total derivatives, since $C(h)$ and $K(h)$ also depend on the variation of pressure head if the flow is unsaturated:

$$\frac{dC(h)}{dP} = \frac{\partial C(h)}{\partial P} + \frac{\partial C(h)}{\partial h}\frac{\partial h}{\partial P} = \frac{\partial C(h)}{\partial P} + \frac{\partial C(h)}{\partial h}\phi \quad (17)$$

$$\frac{dK(h)}{dP} = \frac{\partial K(h)}{\partial P} + \frac{\partial K(h)}{\partial h}\frac{\partial h}{\partial P} = \frac{\partial K(h)}{\partial P} + \frac{\partial K(h)}{\partial h}\phi. \quad (18)$$

[29] Substituting equations (17) and (18) into equation (16) and rearranging, we express the source terms as

$$\left[\frac{\partial C(h,\mathbf{x})}{\partial P} + \omega\frac{\partial S_s}{\partial P}\right]\frac{\partial h}{\partial t} - \left\{\nabla \cdot \left[\frac{\partial K(h,\mathbf{x})}{\partial h}\nabla(h+z)\right] - \frac{\partial C(h)}{\partial h}\frac{\partial h}{\partial t}\right\}\phi - \frac{\partial K(h)}{\partial h}\nabla(h+z)\nabla\phi - \nabla \cdot \left(\frac{\partial K(h)}{\partial P}\nabla(h+z)\right). \quad (19)$$

[30] The expression in the curly brackets before ϕ in equation (19) is zero, since the derivative of equation (1) with respect to h is always zero. Thus, equation (19) becomes

$$\left[\frac{\partial C(h,\mathbf{x})}{\partial P} + \omega\frac{\partial S_s}{\partial P}\right]\frac{\partial h}{\partial t} - \frac{\partial K(h)}{\partial h}\nabla(h+z)\nabla\phi - \nabla \cdot \left[\frac{\partial K(h)}{\partial P}\nabla(h+z)\right]. \quad (20)$$

[31] Replacing the right-hand side of equation (16) with equation (20), we have the final sensitivity equation for flow under variably saturated condition:

$$\nabla \cdot [K(h,\mathbf{x})\nabla\phi] - [\omega S_s + C(h)]\frac{\partial \phi}{\partial t} + \frac{\partial K(h)}{\partial h}\nabla(h+z)\nabla\phi = \left[\frac{\partial C(h,\mathbf{x})}{\partial P} + \omega\frac{\partial S_s}{\partial P}\right]\frac{\partial h}{\partial t} - \nabla \cdot \left[\frac{\partial K(h)}{\partial P}\nabla(h+z)\right]. \quad (21)$$

[32] The left-hand side of equation (21) has the same form as the variably saturated governing equation with an additional advection-like term, which exists only in the unsaturated region. The term on the right-hand side is the source/sink. The sensitivity equations are linear and can be solved without iteration.

[33] One boundary condition for equation (21), which corresponds to the constant head boundary for equation (1), is

$$\phi|_{\Gamma_1} = 0. \quad (22)$$

[34] The boundary condition corresponding to the prescribed flux boundary for equation (1) can be obtained by taking the derivative of the flux boundary condition with respect to the parameter:

$$\frac{\partial}{\partial P}[K(h)\nabla(h+z)] = \frac{\partial q}{\partial P}. \quad (23)$$

[35] We have

$$\left[\frac{\partial K(h)}{\partial P} + \frac{\partial K(h)}{\partial h}\phi\right]\nabla(h+z) + K(h)\nabla\phi = 0, \quad (24)$$

and equation (24) can be written as

$$q_{\text{sensitivity}} = K(h)\nabla\phi = -\frac{\partial K(h)}{\partial h}\nabla(h+z)\phi - \frac{\partial K(h)}{\partial f}\nabla(h+z). \quad (25)$$

[36] The flux boundary associated with the flow equation is thus changed into a type 3 boundary. *Huyakorn and Pinder* [1983] suggest a method for discretizing and incorporating this equation.

2.3.2. Adjoint State Approach

[37] For calculating the sensitivity of the head with respect to parameters in the heterogeneous model, the adjoint state method is more computationally efficient than the sensitivity equation approach. The detailed derivation of the adjoint equation can be found in *Li and Yeh* [1998]. The adjoint state equation corresponding to equation (1) is

$$\begin{aligned} &\nabla\cdot[K(h,\mathbf{x})\nabla\Phi] - [C(h,\mathbf{x}) + \omega S_s]\frac{\partial\Phi}{\partial t} - \frac{\partial K(h,\mathbf{x})}{\partial h}\nabla(h+z) \\ &\nabla\Phi = -\delta(\mathbf{x}-\mathbf{x}_k)(t-t_l) \end{aligned} \quad (26)$$

subject to boundary and final time conditions:

$$\begin{aligned} \Phi = 0 \quad &\text{at} \quad t = t_{\text{final}} \\ \Phi = 0 \quad &\text{at} \quad \Gamma_1 \\ K(h,\mathbf{x})\nabla\Phi = 0 \quad &\text{at} \quad \Gamma_2, \end{aligned} \quad (27)$$

where Φ is the adjoint variable. The equation is linear in terms of the adjoint variable and is very similar to the sensitivity equation (equation (21)) except the source term on the right side becomes the Kronecker delta function. The $\mathbf{x}_k$ and t_l in the delta function are the head observation location and time. Equation (26) must be solved backward in time. For flow in fully saturated media, t_{final} can be set to the last observation time of drawdown-time data at a given observation location, and then equation (26) can be solved by marching backward to time zero, This result can be saved for other observation times. On the other hand, for flow in unsaturated or variably saturated media, equation (26) must be solved for each observation time at a given observation location. Accordingly, if the number of temporal observations increases, the computational cost can increase significantly. As a result, an optimal temporal sampling strategy for analysis of HT surveys in an unconfined aquifer is essential.

[38] The sensitivity for the heterogeneous media is then calculated by integration of adjoint variable, for example,

$$\frac{\partial h(\mathbf{x}_k, t_l)}{\partial \ln K_S(\mathbf{x}_n)} = \int_T \int_{\Omega_n} -K(h,\mathbf{x})\nabla\Phi\nabla(h+z)\,\mathrm{d}\Omega\mathrm{d}t. \quad (28)$$

[39] It represents the sensitivity of head at location $\mathbf{x}_k$ and time t_l with respect to log hydraulic conductivity $f(\mathbf{x}_n)$ at location $\mathbf{x}_n$. When the number of spatial and temporal head observations is less than the number of parameters, the adjoint state approach is unequivocally efficient.

3. Numerical Experiments

[40] We use the following numerical experiments to illustrate the behavior of the cross correlations between observed heads and hydraulic parameters in homogeneous and heterogeneous synthetic aquifers. The configurations and parameter values are similar to those studies by *Nwankwor et al*. [1992], *Akindunni and Gillham* [1992], and *Moench* [2008] that yielded typical S-shaped drawdown curves during pumping tests in their field unconfined aquifers.

3.1. Homogeneous Media

[41] For the homogeneous synthetic aquifer, we employed a 2-D axisymmetric cross-sectional forward equation and the sensitivity equation for simulating evolution of drawdown and calculating cross correlations for the sake of computational efficiency. The 2-D axisymmetric model had a radius (r) of 100 m and a height of 9 m. Before pumping, the pressure head was hydrostatic with the water table located at $z = 6$ m. A well was represented as a point sink located at $r = 0$ m, $z = 1$ m. The top, bottom, and sides of the aquifer were assigned as no-flux boundaries. The domain was discretized into 2935 mixed triangular and rectangular elements with finer elements near the pumping well and the initial water table. Pumping from the well was simulated for 1000 min at a rate of 0.01 m^3/min. No noticeable head changes were observed near the boundary at the end of the pumping test. The drawdowns anywhere in the aquifer were essentially not affected by the boundaries. Three observation points at elevations $z = 1$ and 4 m (in the saturated zone), and $z = 7$ m (in the vadose zone) at radius $r = 6$ m were selected to collect drawdown data.

[42] The parameters of the Gardner and Russo model for unsaturated hydraulic conductivity curve and moisture release curve were as follows: $K_S = 0.004$ m/min, $S_S = 0.0005$/m, $\alpha = 8$/m, $\theta_S = 0.37$ and $\theta_r = 0.07$. The variance of every parameter required in the calculation of cross correlation was assumed to be one. Different variances could have been assigned to different parameters to emphasize its overall importance.

3.2. Heterogeneous Media

[43] Analysis of the cross correlation in heterogeneous media requires the use of a fully three-dimensional (3-D) model because of the nonsymmetric features of cross correlations as explained in section 4.2. This 3-D model had a dimension 200 m × 200 m × 9 m to maintain consistency with the 2-D axisymmetric model used for the homogenous aquifer. The model domain was discretized into 380,880 finite elements. Near the water table (from $z = 6$ to 7.5 m), a vertical discretization of 0.2 m was used, and a discretization of 0.5 m was used from $z = 0$ to 6 m and from $z = 7.5$ to 9 m. In the horizontal direction, the size of the mesh was 0.5 m from $x = 76$ to 124 m and $y = 76$ to 124 m and was 4 m otherwise. The pumping well was located in the center of the domain at $x = 100$ m, $y = 100$ m and $z = 1$ m. Three selected observation locations in the 3-D model corresponded to observation locations in the 2-D axisymmetric

model. They were located at $x = 106$ m, $y = 100$ m in the x-y plane and $z = 1$, 4, and 7 m in the vertical direction.

[44] Mean parameter values and unsaturated constitutive models used for the 3-D heterogeneous model were identical to those used in the 2-D homogeneous model. The correlation scales for K_S, S_S, α, and θ_S were 2 m in horizontal direction and 0.5 m in the vertical direction. A unit variance was assigned to each parameter for convenience and without loss of generality.

3.3. Numerical Code

[45] The variably saturated governing equation (equation (1)) is similar to the sensitivity equation (equation (21)) and the adjoint state equation (equation (26)). As a result, only minor revisions of the forward model are needed to calculate sensitivity. The calculation of sensitivity equations for different hydraulic parameters and adjoint state equations for different observations is independent of each other. A parallel computational algorithm can be easily implemented by Message Passing Interface (MPI) [*Gropp et al*., 1999]. The implementation of this parallel computational algorithm can expedite the computation for the cross-correlation analysis as well as the joint interpretation of sequential pumping tests to be discussed in D. Mao et al. (Joint interpretation of sequential pumping tests in unconfined aquifers, submitted to *Water Resources Research*, 2012). The existing groundwater forward model codes VSAFT2 [*Yeh et al*., 1993] and (Variably Saturated Flow and Transport in 2-D) [*Srivastava and Yeh*, 1992] were revised to incorporate these changes.

4. Results and Discussion

4.1. Homogeneous Media

[46] The temporal evolutions of the cross correlation between the parameters, K_S, S_S, α, and θ_S of the homogeneous medium (section 3.1) and the heads at a radial distance ($r = 6$ m) and elevations ($z = 1$ and 4 m) in the saturated zone are illustrated in Figures 1a and 1b. The cross correlations between these parameters and the head in the vadose zone at $r = 1$ m and $z = 7$ m are shown in Figure 1c as a function of time. Besides the cross correlations, we also plot the drawdown (s) with time as a blue solid curve in Figures 1a, 1b, and 1c corresponding to each observation location.

[47] Generally speaking, the temporal evolutions of the cross correlation between the heads at the two elevations in the saturated zone with the parameters are similar, but the timings of the cross correlations at the higher elevation are delayed slightly. As illustrated in Figures 1a and 1b, the drawdown-log time curves at these two elevations exhibit the typical S-shaped response of an unconfined aquifer due to pumping. That is, at early times, drawdown rises rapidly, then it slows down at intermediate times, and, at late times, it rises rapidly again. The exact times of the three time periods would vary with many factors. We therefore discuss the behaviors of the cross correlations based on the early, intermediate, and late times of the two S-shaped drawdown-time curves in the following sections.

4.1.1. Early Times ($t < 5$ min)

[48] At these times, flow to the pumping well is mainly from release of water from the storage in the saturated region within radial distances between the pumping well and observation locations. Therefore, if the head at the observation location is high (i.e., the hydraulic gradient is steep toward the pumping well), the K_S of the aquifer is, therefore, likely low and vice versa. Note that the qualifier, "likely," is used to emphasize effects of uncertainty in observed heads due to measurement errors as well as spatial variability. The observed heads in the saturated zone are thus negatively correlated with K_S.

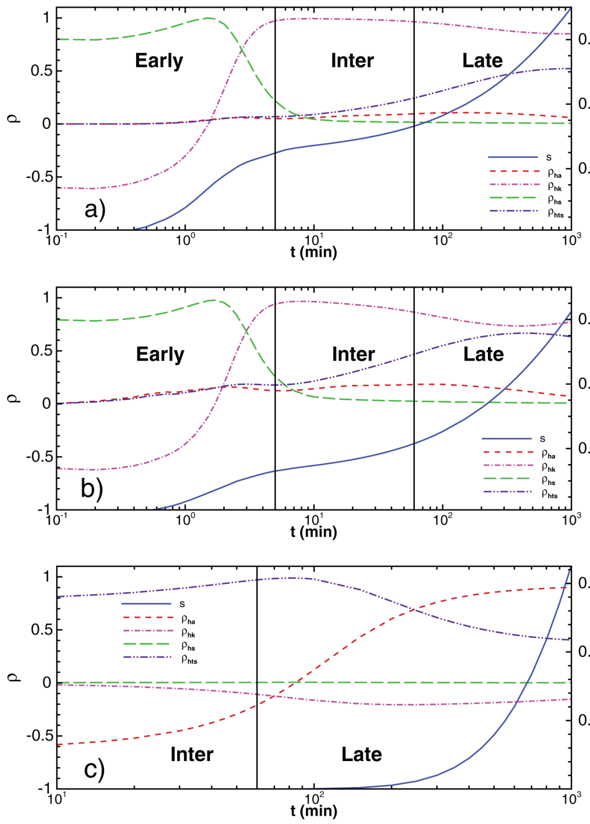

Figure 1. Cross correlation as a function of t between K_S, S_S, α, and θ_S of homogeneous media and observed heads at $r = 6$ m and (a) $z = 1$ m, (b) $z = 4$ m (both are in the saturated zone), and (c) $z^* = 7$ m (in the vadose zone). The blue solid lines represent the drawdown, s. Two vertical lines separate the curves into early, intermediate (inter), and late time periods.

[49] Aquifer compaction and water expansion are major mechanisms responsible for the water release from the storage in the region at this time period, and they are represented by the parameter S_S. The larger the S_S, the more water can be released per unit drawdown, resulting in the smaller drawdown (higher head) at the observation well for a given amount of release. The head in the saturated zone is, thus, positively correlated with S_S. This cross correlation reaches the maximum around this time and decreases afterward. As expected, effects of parameter α and θ_S on the heads in the saturated zone are small. Their effects are greater on the head observed close to the vadose zone. Overall, there is no pressure response at the observation location in the vadose zone at this time period.

4.1.2. Intermediate Times (5 min $\leq t \leq$ 60 min)

[50] At the intermediate times, the rate of drawdown at the observation locations starts to decrease, and the flat portion of the S-shaped drawdown-time curve in the saturated

zone is formed. Water flowing to the pumping well is now mainly from drainage of the vadose zone and drainage of pores due to lowering of the water table at locations above the elevations of the two head measurement locations in the saturated zone. The zero cross correlation between the heads and S_S at these two locations at this time period further confirms this fact.

[51] Because flow is from locations above the observation location, if the observed head is higher (or smaller drawdown) than the one simulated with the mean parameter value, then the hydraulic gradient behind the observation location is likely smaller than the simulated, and, thus, the aquifer likely has a larger value of K_S than the mean value. The cross correlation between the head in the saturated zone and K_S is, thus, positive.

[52] However, the cross correlation between the head in the vadose zone and K_S is negative and small (less than -0.3). Such a negative correlation implies that if the head in the vadose zone is less negative (near saturation), then the K_S value is likely to be small such that little water is drained. Pressure head responses at the measurement point in the vadose zone are also insignificant (Figure 1c). This implies that the head measurement at this time and location may carry little formation about the K_S value of the aquifer.

[53] The impacts of aquifer parameters α and θ_S on the heads in the saturated zone increase during this time period as shown in Figures 1a and 1b. The cross correlation between heads and θ_S is higher than that of α, although both values are small.

4.1.3. Late Times ($t > 60$ min)

[54] The rate of drawdown change at this time period at the two observation locations in the saturated zone begins to increase to form the second rising limb of the S-shaped drawdown-time curves. Drawdown observed at the sample location in the vadose zone increases significantly. The positive correlation between K_S and the heads at the two locations in the saturated zone decreases slightly but remains high. The head measurement in the vadose zone becomes more negatively correlated with K_S (Figure 1c). On the other hand, S_S does not correlate with any of these three heads, reflecting the fact that flow near these observation locations approaches a steady-state condition.

[55] At this time period, the positive relationship between the head at the two measurement points in the saturated zone and θ_S is increasing greatly. This positive correlation means that the larger the value of θ_S, the more water can be released from vadose zone drainage and pore drainage in the initially saturated zone due to lowering of the water table, and the higher heads in the saturated zone. Meanwhile, this correlation with the head in the vadose zone reaches a maximum at the early part of this time period and then decreases, since the pore-size distribution (i.e., α) starts to take effect.

[56] The relationship between α and the heads in the saturated zone increases slightly. Its cross correlation with the head in the vadose zone, however, becomes significantly positive. This positive correlation implies that a larger α (or coarse material) will induce more water released from the dewatering process near the water table, and, thus, a larger (less negative) observed head can be sustained.

[57] Overall, the temporal evolution of the cross correlation between the head at different locations and the parameters (K_S, S_S, α, and θ_S) suggests a temporal data sampling strategy for better estimating the parameters of a homogeneous aquifer. Specifically, drawdown in the saturated zone at early time where the maximum cross correlation takes place will be optimal for estimating the S_S parameter of the aquifer. For the estimation of K_S, using the head measurement from intermediate to late times is the most effective. Although these results are consistent with those by Sun et al. (submitted manuscript, 2012) for the 2-D depth-averaged confined aquifer, our analysis provides new insights for the estimation of parameters in the vadose zone. That is, to derive better estimates of α and θ_S parameters, using head measurements in the vadose zone at late time would be the most appropriate.

[58] In addition, the cross-correlation analysis demonstrates that both α and θ_S control the drainage process in the vadose zone as well as that in the saturated zone resulting from the falling of the water table during the pumping test in unconfined aquifers. This finding is consistent with the results of previous studies by *Nwankwor et al*. [1984] and *Endres et al*. [2006]. They found that pumping test analysis that assumes instantaneous release of water from drainage of pores [*Neuman*, 1972] yields smaller values of θ_S or specific yield (S_y) than those values obtained from core samples. This underestimation is a result of neglecting α in the analysis, which controls the rate of drainage from θ_S.

4.2. Heterogeneous Media

[59] Discussion of the cross-correlation analysis results of heterogeneous media follows the early-time, intermediate-time, and late-time classification used in the homogeneous case. We will show at some selected times in the three time periods the spatial distributions of the cross correlations between the heads at selected measurement locations and each one of the parameters (K_S, S_S, α, and θ_S), the mean drawdown distribution, and the mean streamlines. These plots are along a selected vertical cross section of the aquifer, which cuts through the two observations in the saturated zone, the one in the vadose zone, and the pumping well (section 3.2). Three drawdown contour lines labeled 1, 2, and 3 in these plots denote the drawdown levels of 0.001, 0.012, and 0.15 m. Note that the mean water table, drawdowns and streamline distributions are derived from the mean parameter values, depicting the flow field due to pumping in an equivalent homogeneous unconfined aquifer. In other words, they present the average water table, drawdown, and streamline distributions over an ensemble of heterogeneous aquifers under the same pumping scenarios. They are thus smooth and symmetrical.

4.2.1. Early Times ($t < 5$ min)

4.2.1.1. Cross Correlation Between Heads and K_S

[60] At $t = 0.36$ min, the drawdown due to pumping barely reaches the observation locations in the saturated zone (see Figures 2a and 2b). The cone of depression is mainly confined to the area between the observation wells and the pumping well, and the water table hardly moves. At this time period, water released from the cone of depression due to aquifer compaction and water expansion is the major contributor to the pumping well discharge as indicated in the results for the homogeneous media. Consequently, streamlines are confined to the area encompassing the head observation location and the pumping location.

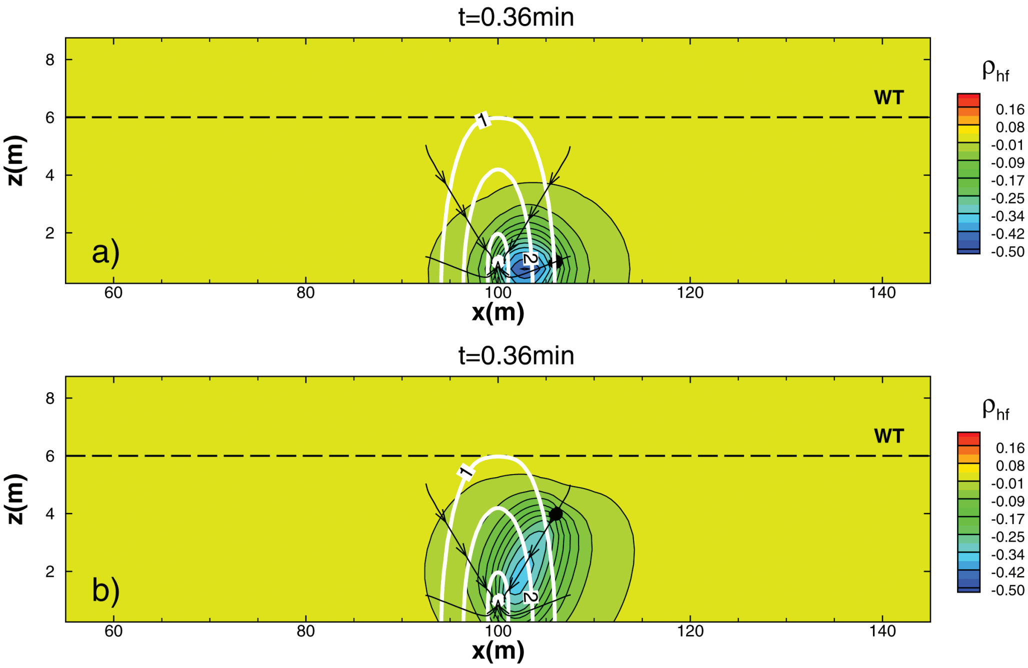

Figure 2. Cross correlation between observed heads at $x = 106$ m, $y = 100$ m with (a) $z = 1$ m and (b) $z = 4$ m (black solid points) and K_S field at $t = 0.36$ min in a cross-section view. The cross section goes through $y = 100$ m, and the pumping well (white solid point) locates at $x = 100$ m, $y = 100$ m, $z = 1$ m. The dashed line shows the location of water table (WT) at the same time. Four black lines with arrows are the streamlines, and the three white solid lines are the drawdown contours with the values 0.001, 0.012, and 0.15 m. z axis is exaggerated for illustration.

[61] Consider the streamline passing through the observation location and pumping well. If the head at the observation location along the streamline is higher (or the drawdown is smaller) than the simulated head based on the equivalent homogeneous mean properties, then the hydraulic gradient from the observation location to the pumping well must be higher than that in the homogeneous aquifer. As a result, K_S values downstream of the observation location are likely to be smaller than the mean K_S. This suggests that the head at the observation location is negatively correlated with the K_S field between pumping point and observation points (Figures 2a and 2b). The K_S distribution along adjacent streamlines follows a similar pattern. But this pattern becomes less obvious if the streamline is away from the observation point. Furthermore, this is a 3-D flow converging to the pumping well. As such, 3-D contours of the cross-correlation distribution form a dome. Meanwhile, cross correlation between the head in the vadose zone and K_S everywhere is virtually zero, since there is no noticeable drawdown in the vadose zone.

4.2.1.2. Cross Correlation Between Heads and S_S

[62] Because the elastic property of the aquifer controls the release of water at this time, the head at the observation well in the saturated zone is positively correlated mainly with S_S in the area between the observation well and the pumping well (see Figures 3a and 3b). This area is within the cone of depression (see drawdown contours) that reflects the release of water from the aquifer due to the elastic behavior. The 3-D plot of Figure 3b is illustrated in Figure 10a. Meanwhile, the cross correlation between S_S and the head at the observation point in the vadose zone is virtually zero as expected.

4.2.1.3. Cross Correlation Between Heads and α and θ_S

[63] At this early time period, cross correlation between observed heads at any one of the three observation locations and the unsaturated properties α and θ_S is virtually zero due to inactivity in the vadose zone and the water table.

4.2.2. Intermediate Times (5 min $\leq t \leq$ 60 min)

4.2.2.1. Cross Correlation Between Heads and K_S

[64] At $t = 45$ min, when the observed mean drawdown-time curve in the saturated zone is flatter than that at the other two time periods (Figures 1a and 1b), the cross correlation between heads at the two observation locations in the saturated zone and K_S everywhere in the selected cross-section plane of the aquifer is illustrated in Figures 4a and 4b. As illustrated in Figures 4a and 4b, the cone of depression has already passed the two observation locations and has expanded into the vadose zone. Also, the streamlines originate from locations beyond the observation points and the water table. Furthermore, effects of S_S on the observed heads at the intermediate time period are virtually zero as shown in Figures 1a and 1b, indicating flow in this region is approaching steady-state conditions [also see *Mao et al.*, 2011].

[65] Since the mean flow field symmetrically converges to the pumping well, our discussion will start with two streamlines in the selected plane. The first streamline is the one starting from the vadose (unsaturated) zone, passing through the observation location and then to the pumping well (marked as A in Figure 4a). The second is

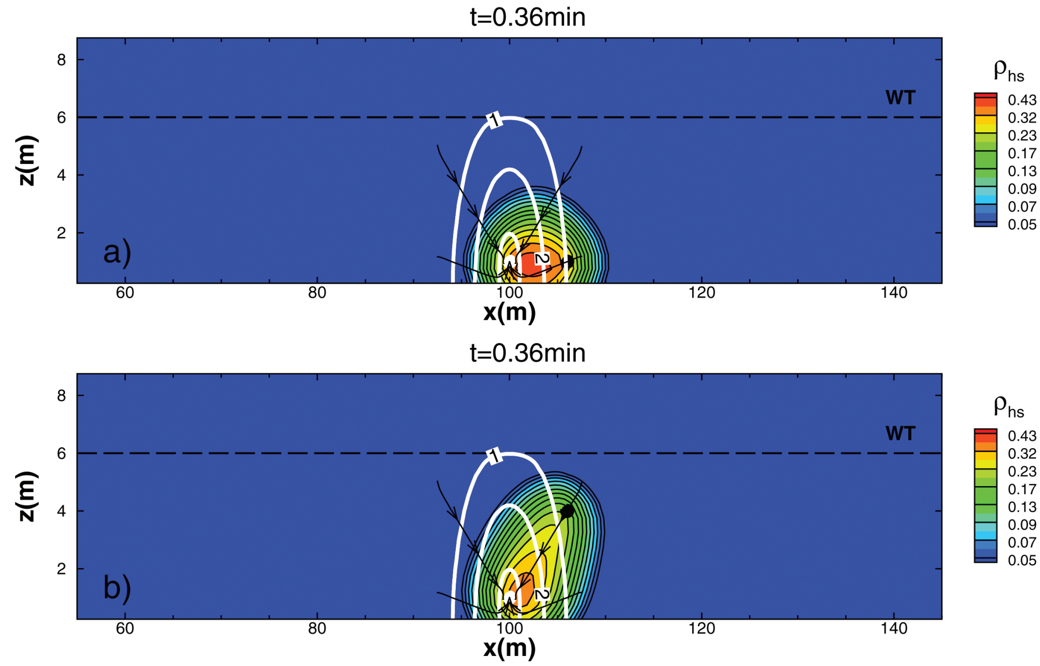

Figure 3. Cross correlation between observed heads at $x = 106$ m, $y = 100$ m with (a) $z = 1$ m and (b) $z = 4$ m (black solid points) and S_S field at $t = 0.36$ min in the selected cross section. The dashed line shows the location of WT at the same time. Four black lines with arrows are the streamlines. The white solid points and three white solids lines are the selected pumping well and drawdown contours, respectively.

the streamline that enters the pumping well from the opposite direction (marked as B in Figure 4a). If the observed head along the first streamline is higher than simulated head based on the mean values of the parameters, the K_S upstream from the observation location along the streamline is likely to be high, and the K_S downstream from the observation location must be low. The opposite is true if the observed head is lower. That is, the head observed at the observation location in the saturated zone has its maximum positive correlation with the K_S some distance (related to correlation scales) upstream of the observation location and has its maximum negative correlation with the K_S some distance downstream along the streamline that passes through the observation port and pumping port.

[66] Now, consider the second streamline. If the K_S along the first streamline between the observation location and pumping well is low, then flux will be smaller than that of the one based on mean K_S. As a consequence, the K_S upstream of the pumping location along the second streamline must be high to maintain the specified well discharge. Therefore, a zone of positive correlation also appears along the streamlines on the opposite side of the observation location.

[67] If the observation location is at the same elevation as the pumping location in the saturated zone, the 3-D correlation contours form a positive correlation cap over the top of the negative correlation cone as illustrated in Figure 4a from the predominantly vertical flow. On the other hand, the cap splits into two parts if the observation point moves to a higher location (upper right of the pumping well; see Figure 4b). The distribution of the cross-correlation values varies with the location of the observation location.

[68] As shown in Figure 4c, the head at the observation location in the vadose zone is weakly and negatively correlated with K_S downstream from the observation point, and there is no corresponding correlation along the second streamline (B). This indicates that this head observation carry only information of heterogeneity in front of the observation location.

4.2.2.2. Cross Correlation Between Heads and S_S

[69] Similar to the homogeneous case (i.e., Figures 1a–1c), S_S everywhere in the aquifer has no significant correlation with the observed heads at the three locations at this time interval.

4.2.2.3. Cross Correlation Between Heads and α and θ_S

[70] Although the cross correlations between the heads in the saturated zone and α are virtually zero at the early time, the heads at the two observation locations in the saturated zone become increasing positively correlated with α ($0.01 - 0.16$) at the vicinity of the water table at $t = 45$ min (Figures 5a and 5b). Physically, this positive correlation implies that if the observed head in the saturated region is higher than the simulated one based on the mean parameters, the parameter α at the vicinity of the water table must be large (coarse materials) such that large amount of water can be released rapidly to sustain the high heads. The head in the vadose zone is negatively correlated with the α values around the observation location (Figure 5c). This is consistent with its behavior in Figure 1c.

[71] The cross correlations between the heads at the three locations and θ_S everywhere in the aquifer are illustrated in

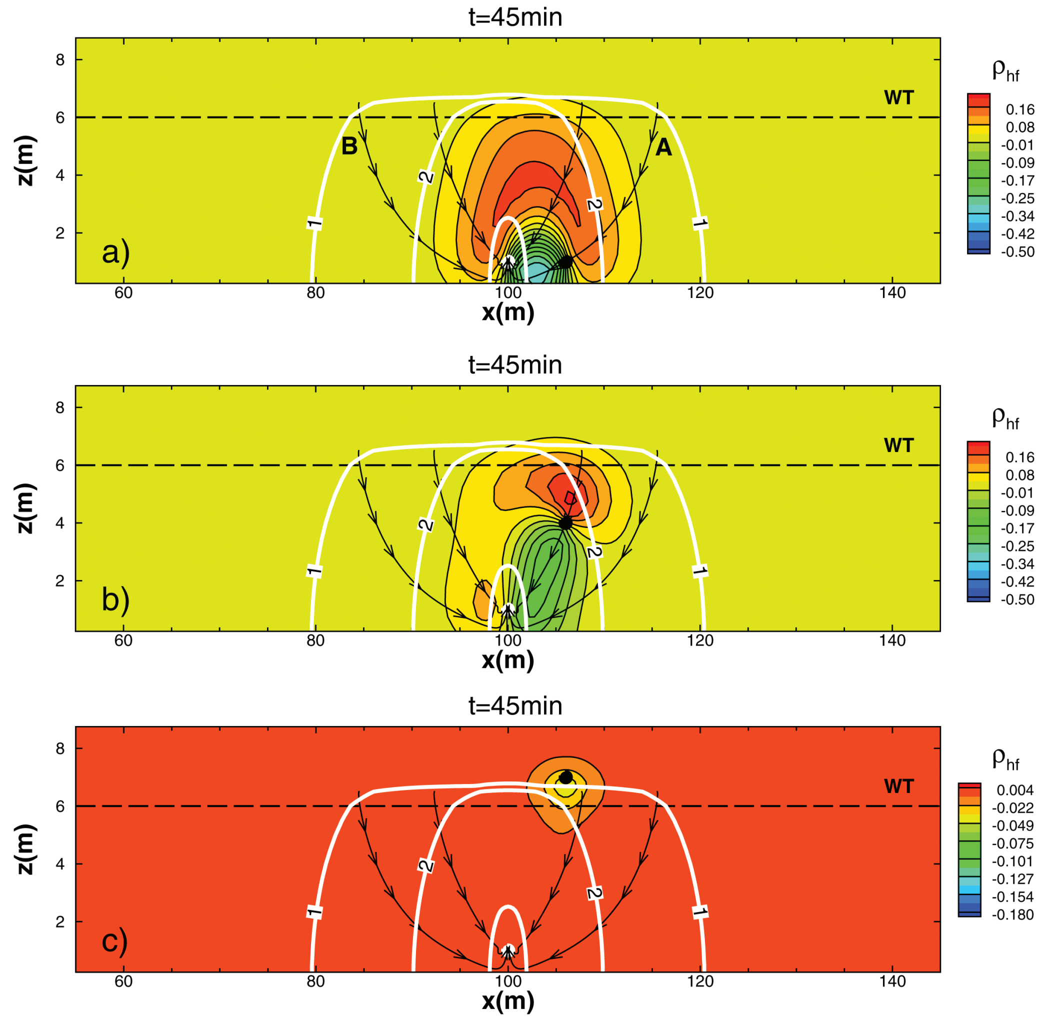

Figure 4. Cross correlation between observed heads at $x = 106$ and 100 m with (a) $z = 1$ m, (b) $z = 4$ m, and (c) $z = 7$ m (black solid points) and K_S field at $t = 45$ min in the selected cross section. The dashed line shows the location of WT at the same time. Four black lines with arrows are the streamlines. The white solid points and three white solids lines are the selected pumping well and drawdown contours, respectively. Different legend has to been used for the well in the vadose zone, since it has a different range of variation. Streamlines A and B in Figure 4a are those discussed in the text.

Figures 6a–6c. Although the spatial patterns of the cross correlations are similar to those of α in Figures 5a–5c, their values are positive and larger than those for α and consistent with those shown in Figures 1a–1c. The positive correlation means that the higher a head value is at the observation location, the larger the value of θ_S in the vadose zone. A large θ_S value in the vadose zone ensures that a large amount of water can be released from the drainage of pores to the saturated region to maintain the high head in the saturated region. On the other hand, a less negative head in the vadose zone indicates that the θ_S value of the medium near the head measurement location is probably high.

[72] Notice that, in Figures 5 and 6, nonzero cross correlation between head and unsaturated zone parameters α and θ_S extends below the water table where the medium is saturated. This unique result manifests the effect of the stochastic concept embedded in the cross-correlation analysis. Specifically, the water table shown in Figures 5 and 6 represents the mean water table, whereas the actual water table may be above or below the mean. Because the cross-correlation analysis also considers the correlation scale of the parameter, the knowledge about α and θ_S values in the unsaturated zone thus can be extrapolated below the water table.

4.2.3. Late Times ($t > 60$ min)

4.2.3.1. Cross Correlation Between Heads and K_S

[73] At $t = 900$ min, when the drawdown rises again from the flat portion of the S-shaped drawdown-time curve (see Figures 1a and 1b), the cone of depression expands greatly in lateral directions, and flow to the pumping well becomes more horizontal as shown by the head contours and streamlines in Figures 7a–7c. Similar to the flow field during the intermediate times, streamlines originate from

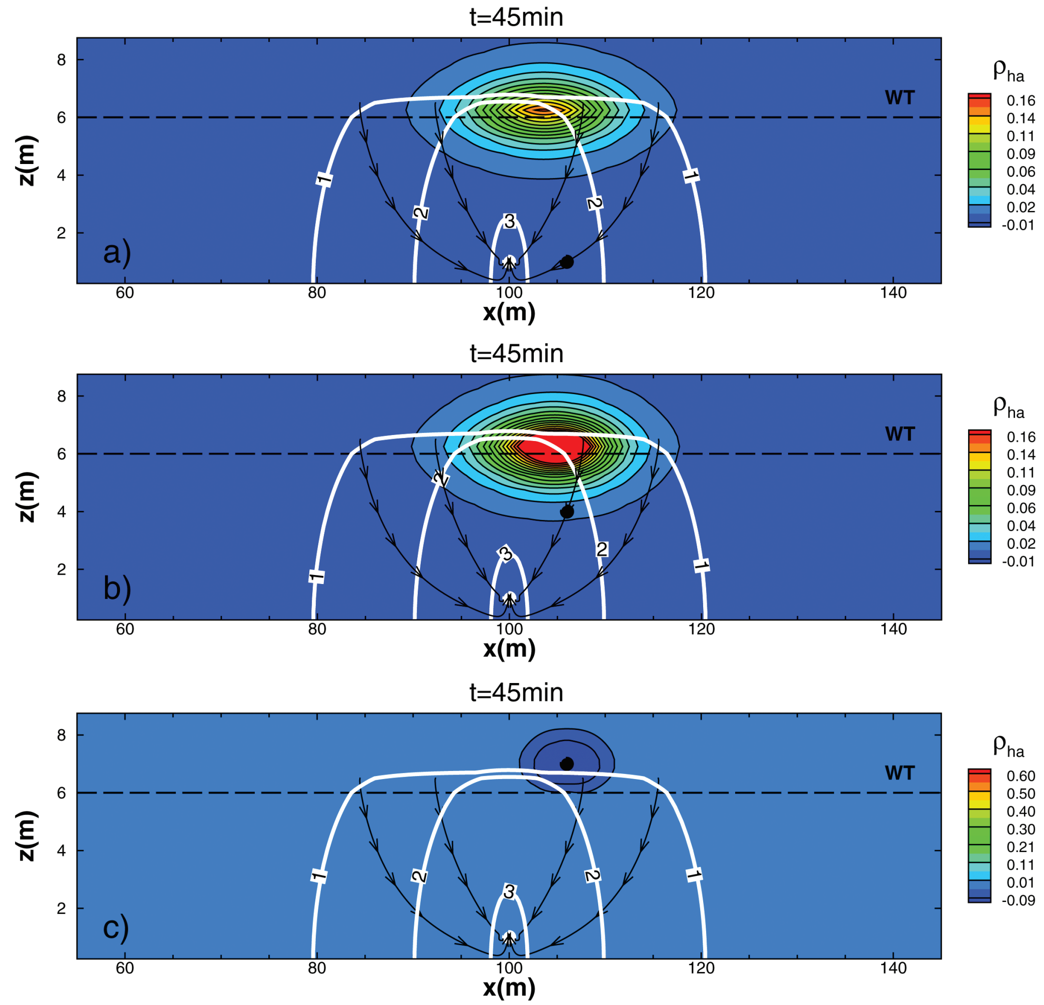

Figure 5. Cross correlation between observed heads at $x = 106$ m, $y = 100$ m with $z = 1$ m, $z = 4$ m, and $z = 7$ m (black solid points) and α field at $t = 45$ min in the selected cross section. The dashed line shows the location of WT at the same time. Four black lines with arrows are the streamlines. The white solid points and three white solids lines are the selected pumping well and drawdown contours, respectively.

locations behind the observation points. Therefore, the head observed at each of the two locations in the saturated zone is positively correlated with the K_S upstream of the observation location and negatively correlated with the K_S downstream along the streamline that passes through the observation port and pumping port. It is also positively correlated with the K_S along the streamline on the opposite side of the pumping well. Since the flow becomes more horizontal, the area of high cross correlation has clearly split into two parts (see Figures 7a and 7b). The distribution of the cross correlation in 3-D, corresponding to Figure 7b, is illustrated in Figure 10b. Notice that the cross correlations are not symmetrical about the pumping well even though the mean flow is.

[74] The cross correlation between the head observed in the vadose zone at this time is negatively correlated with the K_S immediately downstream of the observation location with a limited extent.

4.2.3.2. Cross Correlation Between Heads and S_S

[75] Similar to the homogeneous case (i.e., Figures 1a–1c), S_S everywhere in the aquifer has no significant correlation with the observed heads at the three locations at this time.

4.2.3.3. Cross Correlation Between Heads and α and θ_S

[76] At $t = 900$ min, the correlations of parameter α with the heads in the saturated zone expand to greater areas near the water table in comparison with those at $t = 45$ min, but their values decrease (Figures 8a–8c). Its correlation with the head in the vadose zone becomes positive and increases significantly. The 3-D plot corresponding to Figure 8b is shown in Figure 10c.

[77] The heads at the two locations in the saturated zone are again positively correlated with θ_S over greater areas in the vadose zone right above the pumping location. A 3-D plot of the correlation corresponding to Figure 9b is shown in Figure 10d. The head in the vadose zone is also positively correlated with this parameter, but the area of influence remains similar to that at $t = 45$ min.

4.3. Effect of Correlation Scale

[78] The cross correlation between the observed head and the selected parameter everywhere in the aquifer

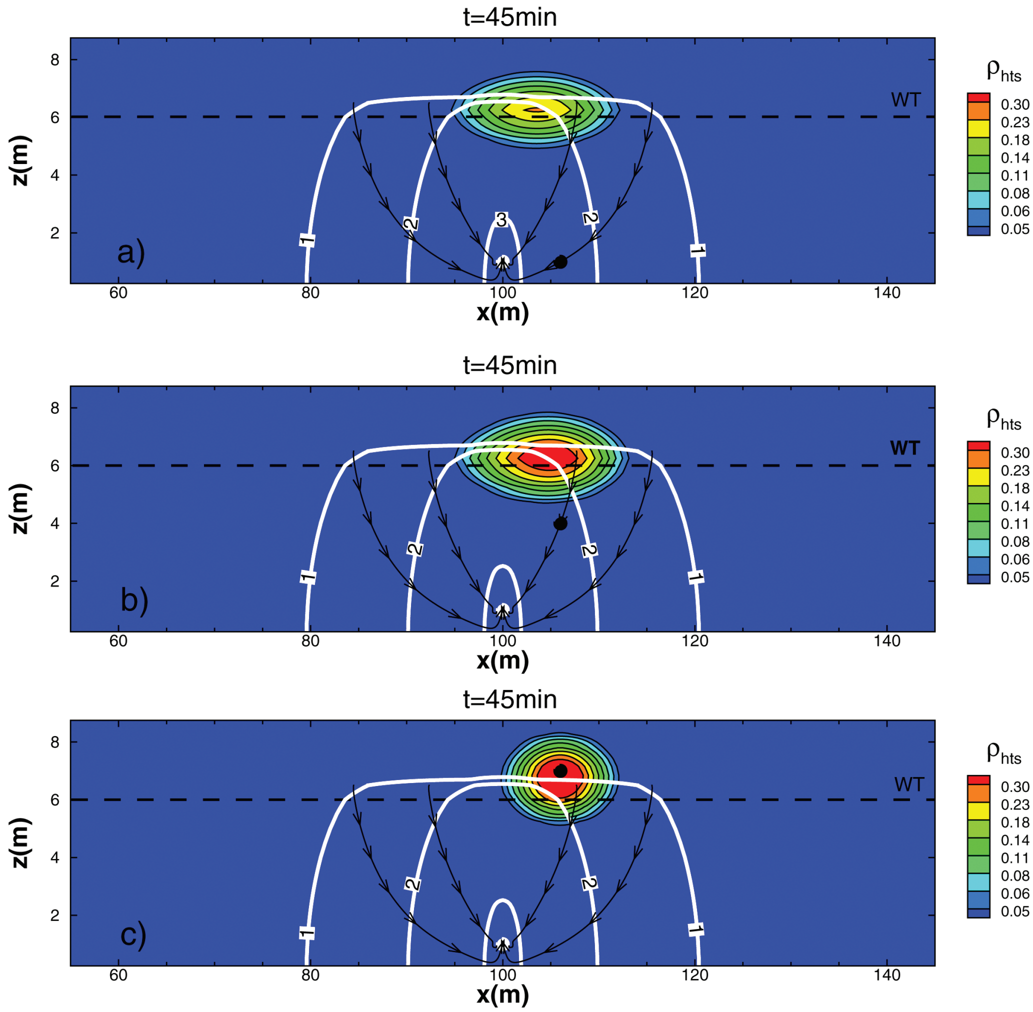

Figure 6. Cross correlation between observed heads at $x = 106$ m, $y = 100$ m with $z = 1$ m, $z = 4$ m, and $z = 7$ m (black solid points) and θ_S field at $t = 45$ min in the selected cross section. The dashed line shows the location of WT at the same time. Four black lines with arrows are the flow lines. The white solid points and three white solids lines are the selected pumping well and drawdown contours, respectively.

depends on the covariance functions of the 3-D heterogeneity (equations (12)–(14)). The cross correlations between the observation well at ($z = 4$ m, $r = 6$ m) and parameters K_S at three different times are shown in Figures 11a–11c when the horizontal correlation scales are increased from 2 to 20 m. Overall, the cross correlation preserves the general pattern of Figures 2b, 4b, and 7b in time and space. But the pattern elongates reflecting the longer correlation scale in horizontal direction. Cross-correlation contour maps for other parameters follow the same principle with larger correlation scales in the horizontal direction. This result implies that the observed head carries information about the parameter over greater horizontal areas.

4.4. Principle of Reciprocity

[79] The cross-correlation analysis for the heterogeneous aquifer reveals information about the heterogeneity that could be extracted from observed heads at an observation well during a pumping test. According to the analysis, observation wells at different locations may carry nonredundant information. Furthermore, by changing the position of pumping and observation locations in an existing well field (i.e., HT, *Yeh and Liu* [2000], *Zhu and Yeh* [2005], and others), we could potentially obtain more information about heterogeneity of the aquifer than using single pumping well. The principle of reciprocity [*Bruggeman*, 1972] however suggests that some of the information in confined aquifers is redundant. That is, responses at location B to an excitation at location A are identical to the response at location A to an equivalent response at location B. This is mathematically true for a confined aquifer for both homogeneous and heterogeneous media. *Delay et al.* [2011] challenged this principle in the dual-continuum media. To the best of our knowledge, the validity of the principle under variably saturated condition has never been addressed.

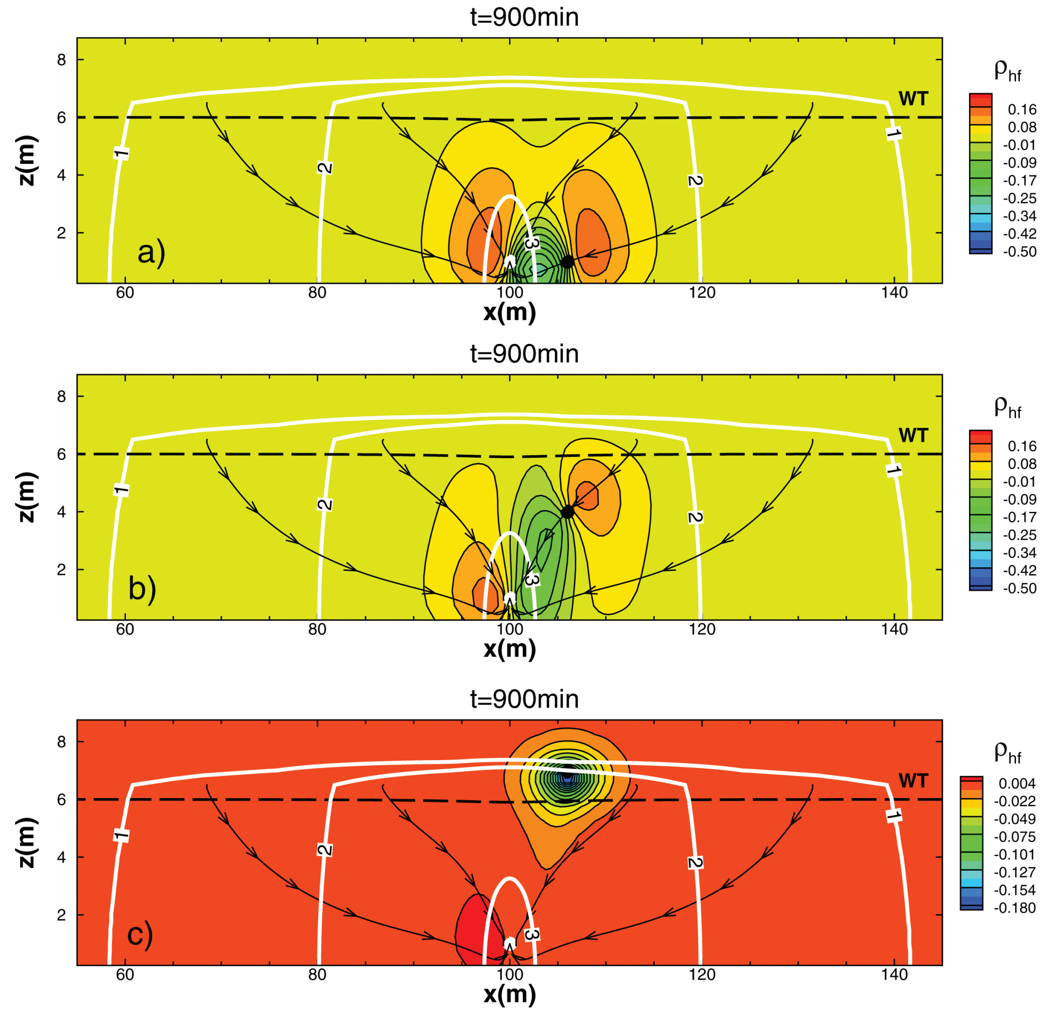

Figure 7. Cross correlation between observed heads at $x = 106$ m, $y = 100$ m with $z = 1$ m, $z = 4$ m, and $z = 7$ m (black solid points) and K_S field at $t = 900$ min in the selected cross section. The dashed line shows the location of WT at the same time. Four black lines with arrows are the streamlines. The white solid points and three white solids lines are the selected pumping well and drawdown contours, respectively.

[80] We conducted a series of numerical simulation experiments to examine the validity of the principle of reciprocity for flow in variably saturated media. In these experiments, the existing pumping location ($x = 100$ m, $y = 100$ m, and $z = 1$ m) is named as point 1 and three observation locations: points 2, 3, and 4 at $z = 1$, 4, and 7 m, $x = 106$ m, and $y = 100$ m, respectively. We then added another point observation near the water table ($z = 5.5$ m, $x = 106$ m, and y=100 m) that is point 5. Instead of pumping water out of the pumping location, we injected water to avoid numerical convergence problems caused by nonlinear nature of the unsaturated flow equation.

[81] First, water was injected at point 1, and heads were observed at points 2–5. As a result, four buildup hydrographs were obtained (i.e., I12, I13, I14, and I15; I stands for injection; the first number denotes the injection well and the second for monitoring well). Afterward, the injection was conducted at points 2–5. During each of these three injections, head responses were recorded at point 1. Similarly, four buildup hydrographs (I21, I31, I41, and I51) were obtained. These four pairs of ISI, (I12, I21), (I13, I31), (I14, I41), and (I15, I51), are plotted in Figure 12 as a function of time.

[82] If the injection point and monitoring point are at the same elevation, the pair of head responses at $z = 1$ m (i.e., I12 and I21) is identical. With increasing difference in the elevation of the pair points (e.g., I13 and I31; I15 and I51), differences in head between the pairs at late times become noticeable when the influence of vadose zone becomes effective. For the pair of injection tests at $z = 7$ m (I14 and I41), the head responses are significantly different. Notice

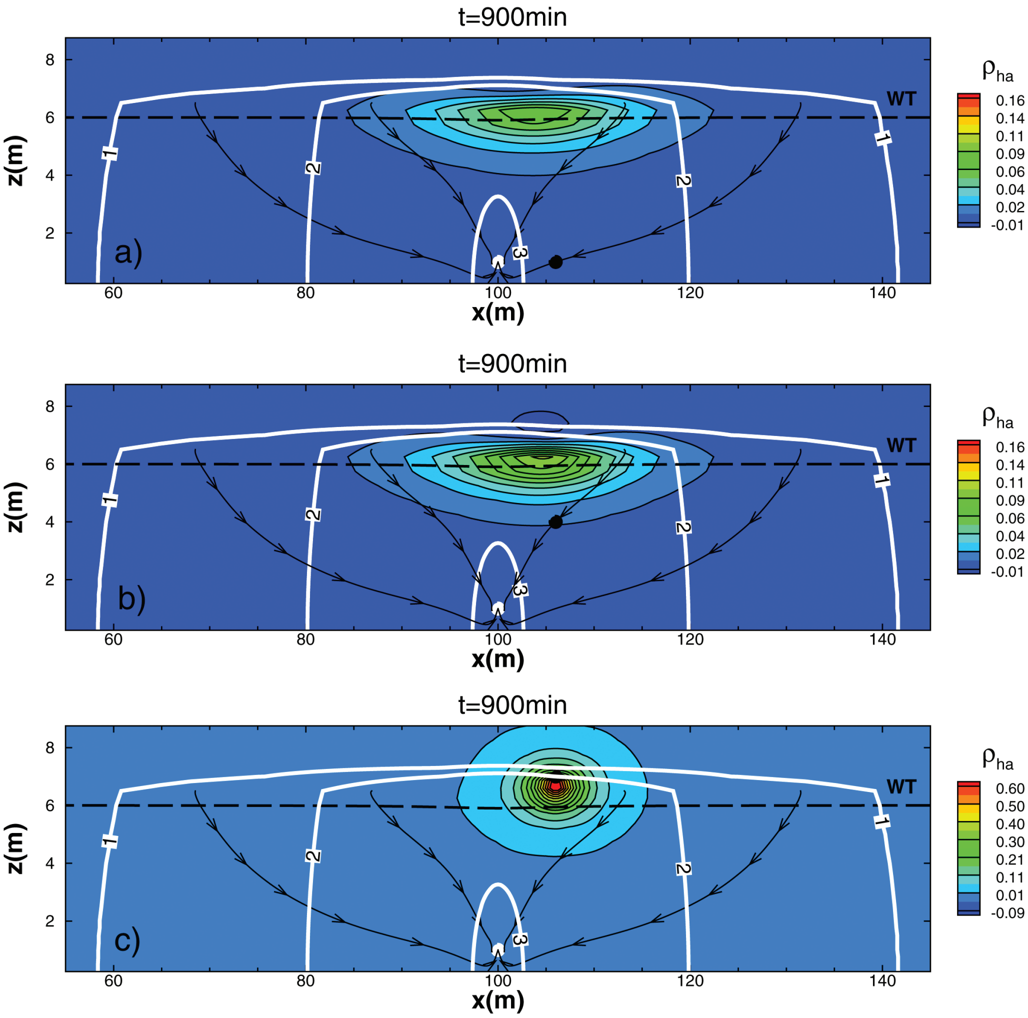

Figure 8. Cross correlation between observed heads at $x = 106$ m, $y = 100$ m with (a) $z = 1$ m, (b) $z = 4$ m, and (c) $z = 7$ m (black solid points) and α field at $t = 900$ min in the selected cross section. The dashed line shows the location of WT at the same time. Four black lines with arrows are the flow lines. The white solid points and three white solids lines are the selected pumping well and drawdown contours, respectively.

that, for I41, the injection point ($z = 7$ m) is in the initial vadose zone, and, for I14, the injection point ($z = 1$ m) is in the saturated zone.

[83] Besides the experiments described here, we also conducted numerous tests with homogeneous and heterogeneous assumptions under one-dimensional, 2-D, or 3-D variably saturated flow conditions. The results from all these numerical experiments indicate that principle of reciprocity does not hold under the variably saturated condition if vertical flow is involved when the pair of points is not on the same elevation.

[84] The nature of the governing equation for flow through 3-D variably saturated porous media (equation (1)) may by itself explain these findings. To show this, we will decompose the equation into two parts: one for the vadose zone

$$\nabla \cdot [K(h, \mathbf{x})\nabla h] + \frac{\partial K(h, x)}{\partial h}\frac{\partial h}{\partial z} + Q(\mathrm{x}_p) = C(h, \mathbf{x})\frac{\partial h}{\partial t}, \qquad (29)$$

and the other for the saturated zone

$$\nabla \cdot [K(\mathbf{x})\nabla h] + \frac{\partial K(\mathbf{x})}{\partial z} + Q(\mathrm{x}_p) = S_s(\mathbf{x})\frac{\partial h}{\partial t}. \qquad (30)$$

[85] In the saturated zone, the governing equation (equation (30)) is a linear diffusion equation with a sink or source term. Thus, the principle of reciprocity in the saturated zone is always true. On the other hand, the governing flow equation for the vadose zone (equation (29)) is a nonlinear advection-diffusion equation in terms of h. The

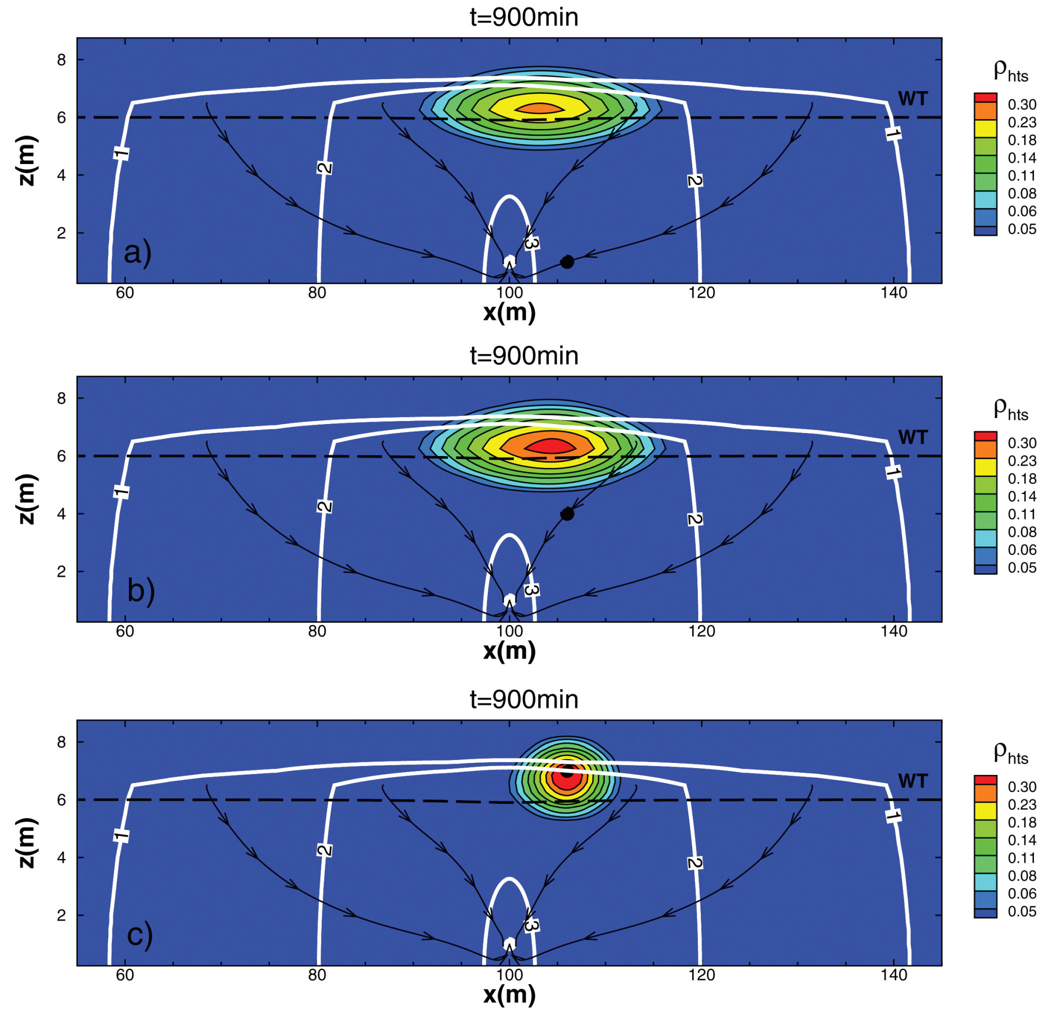

Figure 9. Cross correlation between observed heads at $x = 106$ m, $y = 100$ m with (a) $z = 1$ m, (b) $z = 4$ m, and (c) $z =$ and 7 m (black solid points) and θ_S field at $t = 900$ min in the selected cross section. The dashed line shows the location of WT at the same time. Four black lines with arrows are the flow lines. The white solid points and three white solids lines are the selected pumping well and drawdown contours, respectively.

second term on the left of the equation is the gravity term, which represents advection due to gravity with the velocity, $\partial K(h,\mathrm{x})/\partial h$. Addition of this vertical downward velocity to the symmetric diffusion process and the dependence of hydraulic conductivity on head will lead to different flow fields and thus different observed responses for any pair of injection-monitor locations at different elevations. This explains the greater deviations from the principle of reciprocity near the water table ($z = 4$ and 5.5 m) or in the vadose zone ($z = 7$ m). In other words, the principle of reciprocity does not hold for pumping tests in unconfined aquifers unless the pair of wells is at the same elevation. Although we did not show the cross correlation for these cases, the outcome is the same as that of the head.

5. Summary and Conclusions

[86] Our cross-correlation analysis of observed heads and hydraulic properties during a pumping test in homogeneous and heterogeneous unconfined aquifers reveals that the head observed in the saturated zone at late times carries the greatest information about K_S heterogeneity

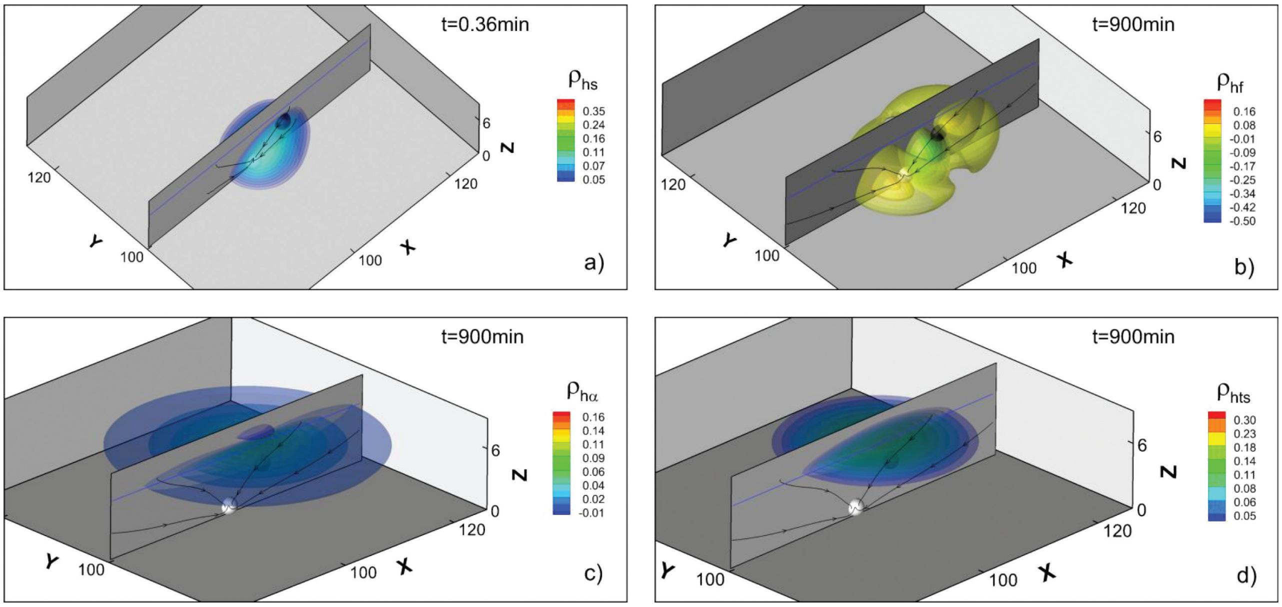

Figure 10. 3-D iso-surfaces contour for parameters (a) S_S, (b) K_S, (c) α, and (d) θ_S, corresponding to Figures 4b, 5b, 7b, and 8b, respectively. The dark cross section is the selected one that goes through $y = 100$ m. The blue solid line is the location of WT, and the four black solid lines with arrows are the flow lines.

distribution. In general, it contains nonsymmetrically weighted information about heterogeneity within the cone of depression. More weight is given to those K_S heterogeneity upstream of the observation location and the region between the observation location and the pumping location along the streamlines passing the observation and pumping locations. Similar weights are also given to those K_S upstream of the pumping well along the streamlines on the opposite side. Although these results are similar to the 2-D depth-averaged confined aquifers, our results reveal complex 3-D spatial distributions of these cross correlations, which challenge previous analyses in confined aquifers by *Bohling* [2009] or *Butler* [1988] using axisymmetric flow models. The information of K_S from head measured at the location in the vadose zone follows similar patterns but is less informative.

[87] Identical to the confined aquifers, the measured head in the saturated zone at the early time carries the most information about S_S heterogeneity in a narrow region along the streamline between the observation and pumping locations.

[88] At intermediate times and late times, the heads measured in the saturated zone largely reflect the heterogeneity of α in the thin unsaturated region near the water table above the pumping and observation locations. The head measured in the vadose zone at late times has the greatest information about α around the observation point in the vadose zone.

[89] Likewise, θ_S has impacts on the head measurements in the saturated zone and the vadose zone during the intermediate and late times. Again, heterogeneity of θ_S in the vadose zone directly above the pumping and monitoring locations has the greatest impact on the head measurement in the saturated zone. Heads measured in the vadose zone correlate well with the heterogeneity of θ_S in the area around their measurement location.

[90] These findings are relevant to the parameter estimation of unconfined aquifers using pumping tests. First of all, results of the cross-correlation analysis of the homogeneous aquifer show that early-time drawdown data in the saturated zone are most suitable for estimating S_S parameter, whereas the drawdown data in the saturated zone at late time are highly desirable for estimating K_S and θ_S. Head data collected in the vadose zone at the late time of the pumping test are a must for the estimation of α.

[91] Second, implications from the cross-correlation analysis of heterogeneous aquifers are significant on the conventional analysis of unconfined aquifer tests. Conventional aquifer analyses rely on drawdown-time data collected at an observation well due to pumping at another well. They also assume aquifer homogeneity for mathematical simplicity [e.g., *Tartakovsky and Neuman*, 2007;

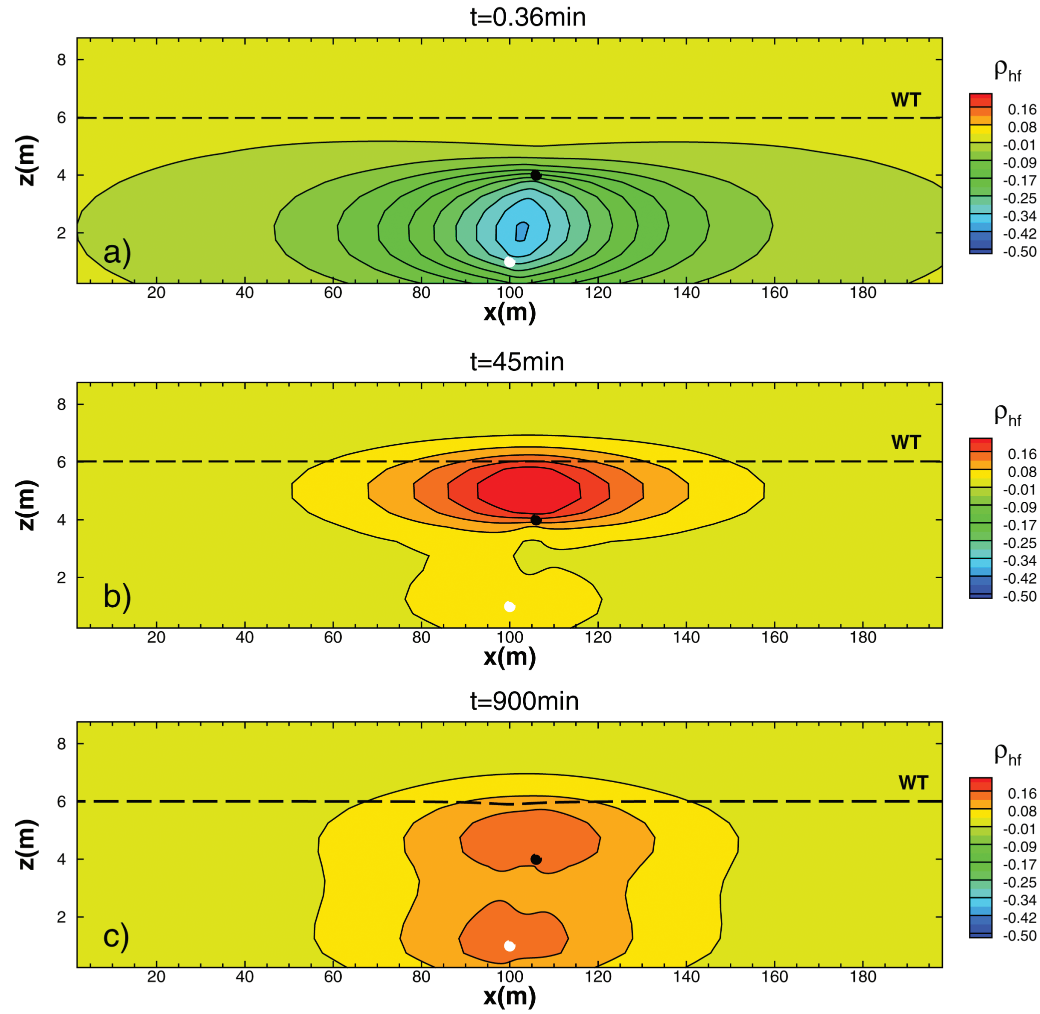

Figure 11. Cross correlation between observed heads at $x = 106$ m, $y = 100$ m, and $z = 4$ m (black solid points) and K_S field at different times (a) 0.36 min, (b) 45 min and (c) 900 min in the selected cross section. The dashed line shows the location of WT at the same time. Four black lines with arrows are the flow lines. The white solid points and three white solids lines are the selected pumping well and drawdown contours, respectively. The correlation scales used here are 20.0, 20.0, and 0.5 m in x, y, and z axes, respectively. A larger range of x axis is used to represent the longer correlation scale.

Moench, 2008; *Mishra and Neuman*, 2010]. The cross-correlation analysis shows that the influences of K_S at different regions of the aquifer on the head at an observation location change with time. As a result, these conventional aquifer analyses will likely lead to ambiguous estimates of aquifer properties as documented by *Wu et al*. [2005], *Straface et al*. [2007], and *Wen et al*. [2010] for confined aquifers. In addition, the unique pattern of the cross correlation between head and hydraulic parameters will likely lead to scenario-dependent estimates of the properties that vary with the location of pumping well as reported by *Huang et al*. [2011] and Sun et al. (submitted manuscript, 2012).

[92] Finally, these complex 3-D cross-correlation patterns between head and parameters may not be representative for all possible scenarios. Nonetheless, they reinforce the need for hydraulic tomography to characterize unconfined aquifers [*Zhu and Yeh*, 2008; *Cardiff and Barrash*, 2011; *Zhu et al*., 2011], or joint interpretation of sequential pumping tests for unconfined aquifer, which is the topic of our next paper (Mao et al., submitted manuscript, 2012). They also supports the call by *Mao et al*. [2011] for the use of 3-D, heterogeneous, variably saturated model for the prediction of aquifer responses as well as parameter estimation in unconfined aquifers. They are also consistent with the results of laboratory experiment by *Berg and Illman* [2012] that applied hydraulic tomography to an unconfined aquifer. At last, our results show that the commonly known principle of reciprocity does not

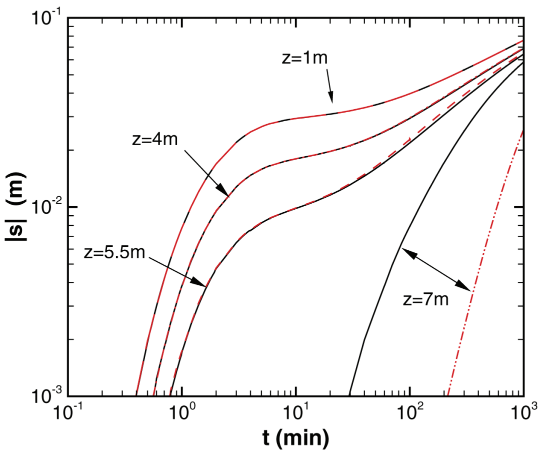

Figure 12. The head buildup $|s|$ hydrographs for the pairs (I12 and I21) at $z = 1$ m; (I13 and I31) at $z = 4$ m; (I14 and I41) at $z = 7$ m; and (I15 and I51) at $z = 5.5$ m. The red lines are the responses of the aquifer at observation points at different elevations due to injection at well 1. The black lines are the responses of the aquifer observed at well 1 due to injection at different elevations.

hold in variably saturated flow that involves vertical flow components.

[93] **Acknowledgments.** This research is supported by NSF grant EAR 1014594. The first author acknowledges the support of "China Scholarship Council." The second author also acknowledges support of the oversea outstanding scholar award of Department of Education, China, through Jilin University, China. Finally, the authors thank Junfeng Zhu, Xiaoyi Liu, and reviewers for their constructive comments.

References

Akindunni, F. F., and R. W. Gillham (1992), Unsaturated and saturated flow in response to pumping of an unconfined aquifer—Numerical investigation of delayed drainage, *Ground Water*, *30*(6), 873–884.

Barker, J. A., and R. Herbert (1982), Pumping tests in patchy aquifers, *Ground Water*, *20*(2), 150–155, doi:10.1111/j.1745-6584.1982.tb02742.x.

Berg, S. J., and W. A. Illman (2011), Three-dimensional transient hydraulic tomography in a highly heterogeneous glaciofluvial aquifer-aquitard system, *Water Resour. Res.*, *47*, W10507, doi:10.1029/2011WR010616.

Berg, S. J., and W. A. Illman (2012), Improved predictions of saturated and unsaturated zone drawdowns in a heterogeneous unconfined aquifer via transient hydraulic tomography: Laboratory sandbox experiments, *J. Hydrol.*, *470–471*, 172–183, http://dx.doi.org/10.1016/j.jhydrol.2012.08.044.

Bohling, G. C. (2009), Sensitivity and resolution of tomographic pumping tests in an alluvial aquifer, *Water Resour. Res.*, *45*, W02420, 1–21, doi:10.1029/2008WR007249.

Boulton, N. (1954), Unsteady radial flow to a pumped well allowing for delayed yield from storage, *Int. Assoc. Sci. Hydrol.*, *37*, 472–477.

Bruggeman, G. (1972), The reciprocity principle in flow through heterogeneous porous media, in *Fundamentals of Transport Phenomena in Porous Media*, edited by IAHR, pp. 136–149, Elsevier, Amsterdam.

Butler, J. J., Jr., (1988), Pumping tests in nonuniform aquifers—The radially symmetric case, *J. Hydrol.*, *101*(1–4), 15–30.

Butler, J. J., Jr., (1990), The role of pumping tests in site characterization: Some theoretical considerations, *Ground Water*, *28*(3), 394–402, doi:10.1111/j.1745-6584.1990.tb02269.x.

Butler, J. J., Jr., and W. Z. Liu (1991), Pumping tests in non-uniform aquifers—The linear strip case, *J. Hydrol.*, *128*(1–4), 69–99, doi:10.1016/0022-1694(91)90132-2.

Butler, J. J., Jr., and W. Z. Liu (1993), Pumping tests in nonuniform aquifers: The radially asymmetric case, *Water Resour. Res.*, *29*(2), 259–269, doi:10.1029/92WR02128.

Butler, J. J., Jr., and C. D. McElwee (1990), Variable-rate pumping tests for radially symmetric nonuniform aquifers, *Water Resour. Res.*, *26*(2), 291–306, doi:10.1029/WR026i002p00291.

Cardiff, M., and W. Barrash (2011), 3-D transient hydraulic tomography in unconfined aquifers with fast drainage response, *Water Resour. Res.*, *47*, W12518, doi:10.1029/2010WR010367.

Dagan, G. (1982), Stochastic modeling of groundwater flow by unconditional and conditional probabilities. 2. The solute transport, *Water Resour. Res.*, *18*(4), 835–848, doi:10.1029/WR018i004p00835.

Delay, F., P. Ackerer, and A. Guadagnini (2011), Theoretical analysis and field evidence of reciprocity gaps during interference pumping tests, *Adv. Water Res.*, *34*(5), 592–606, doi:10.1016/j.advwatres.2011.02.006.

Desbarats, A. J. (1992), Spatial averaging of transmissivity in heterogeneous fields with flow toward a well, *Water Resour. Res.*, *28*(3), 757–767, doi:10.1029/91WR03099.

Desbarats, A. J. (1993), Geostatistical analysis of interwell transmissivity in heterogeneous aquifers, *Water Resour. Res.*, *29*(4), 1239–1246, doi:10.1029/92WR02418.

Endres, A. L., J. P. Jones and E. A. Bertrand (2006), Pumping-induced vadose zone drainage and storage in an unconfined aquifer: A comparison of analytical model predictions and field measurements, *J. Hydrol.*, *335*, 207–218, doi:10.1016/j.jhydrol.2006.07.018.

Gropp, W., E. Lusk, and A. Skjellum (1999), *Using MPI: Portable Parallel Programming with the Message Passing Interface*, 2nd ed., MIT Press, Cambridge, Mass.

Hoeksema, R. J., and P. K. Kitanidis (1984), An application of the geostatistical approach to the inverse problem in two-dimensional groundwater modeling, *Water Resour. Res.*, *20*(7), 1003–1020, doi:10.1029/WR020i007p01003.

Huang, S.-Y., J.-C. Wen, T.-C. J. Yeh, W. Lu, H.-L. Juan, C.-M. Tseng, J.-H. Lee, and K.-C. Chang (2011), Robustness of joint interpretation of sequential pumping tests: Numerical and field experiments, *Water Resour. Res.*, *47*, W10530, doi:10.1029/2011WR010698.

Hughson, D. L., and T.-C. J. Yeh (2000), An inverse model for three-dimensional flow in variably saturated porous media, *Water Resour. Res.*, *36*(4), 829–839, doi:10.1029/2000WR900001.

Hunt, B. (1985), Flow to a well in a multiaquifer system, *Water Resour. Res.*, *21*(11), 1637–1641, doi:10.1029/WR021i011p01637.

Huyakorn, P. S., and G. F. Pinder (1983), *Computational Methods in Subsurface Flow*, 496 pp., Academic, New York.

Illman, W. A., X. Liu, S. Takeuchi, T.-C. J. Yeh, K. Ando, and H. Saegusa (2009), Hydraulic tomography in fractured granite: Mizunami Underground Research site, Japan, *Water Resour. Res.*, *45*(1), W01406, doi:10.1029/2007WR006715.

Indelman, P. (2003), Transient pumping well flow in weakly heterogeneous formations, *Water Resour. Res.*, *39*(10), 1287, doi:10.1029/2003WR002036.

Indelman, P., and G. Dagan (1993a), Upscaling of permeability of anisotropic heterogeneous formations: 2. General structure and small perturbation analysis, *Water Resour. Res.*, *29*(4), 925–933, doi:10.1029/92WR02447.

Indelman, P., and G. Dagan (1993b), Upscaling of permeability of anisotropic heterogeneous formations: 1. The general framework, *Water Resour. Res.*, *29*(4), 917–923, doi:10.1029/92WR02446.

Kitanidis, P. K. (1995), Quasi-linear geostatistical theory for inversing, *Water Resour. Res.*, *31*(10), 2411–2419, doi:10.1029/95WR01945.

Kitanidis, P. K., and E. G. Vomvoris (1983), A geostatistical approach to the inverse problem in groundwater modeling (steady state) and one-dimensional simulations, *Water Resour. Res.*, *19*(3), 677–690, doi:10.1029/WR019i003p00677.

Leven, C., and P. Dietrich (2006), What information can we get from pumping tests?—Comparing pumping test configurations using sensitivity coefficients, *J. Hydrol.*, *319*(1–4), 199–215, doi:10.1016/j.jhydrol.2005.06.030.

Li, B., and T.-C. J. Yeh (1998), Sensitivity and moment analyses of head in variably saturated regimes, *Adv. Water Res.*, *21*(6), 477–485, doi:10.1016/s0309-1708(97)00011-0.

Li, B., and T.-C. J. Yeh (1999), Cokriging estimation of the conductivity field under variably saturated flow conditions, *Water Resour. Res.*, *35*(12), 3663–3674, doi:10.1029/1999WR900268.

Mao, D., L. Wan, T.-C. J. Yeh, C.-H. Lee, K.-C. Hsu, J.-C. Wen, and W. Lu (2011), A revisit of drawdown behavior during pumping in unconfined aquifers, *Water Resour. Res.*, *47*, W05502, doi:10.1029/2010WR009326.

Mathias, S. A., and A. P. Butler (2006), Linearized Richards' equation approach to pumping test analysis in compressible aquifers, *Water Resour. Res.*, *42*, W06408, doi:10.1029/2005WR004680.

McElwee, C. D. (1987), Sensitivity analysis of groundwater models, in *Advances in Transport Phenomena in Porous Media*, edited by J. Bear and M. Y. Carapcioglu, pp. 751–817, Noordhoff Int. Publ., Leiden.

Mishra, P. K., and S. P. Neuman (2010), Improved forward and inverse analyses of saturated-unsaturated flow toward a well in a compressible unconfined aquifer, *Water Resour. Res.*, *46*, W07508, doi:10.1029/2009WR008899.

Moench, A. F. (1997), Flow to a well of finite diameter in a homogeneous, anisotropic water table aquifer, *Water Resour. Res.*, *33*(6), 1397–1407, doi:10.1029/97WR00651.

Moench, A. F. (2008), Analytical and numerical analyses of an unconfined aquifer test considering unsaturated zone characteristics, *Water Resour. Res.*, *44*, W06409, doi:10.1029/2006WR005736.

Naff, R. L. (1991), Radial flow in heterogeneous porous media: An analysis of specific discharge, *Water Resour. Res.*, *27*(3), 307–316, doi:10.1029/90WR02410.

Narasimhan, T., and M. Zhu (1993), Transient flow of water to a well in an unconfined aquifer: Applicability of some conceptual models, *Water Resour. Res.*, *29*(1), 179–191, doi:10.1029/92WR01959.

Neuman, S. P. (1972), Theory of flow in unconfined aquifers considering delayed response of the water table, *Water Resour. Res.*, *8*(4), 1031–1045, doi:10.1029/WR008i004p01031.

Neuman, S. P., and S. Orr (1993), Prediction of steady state flow in nonuniform geologic media by conditional moments: Exact nonlocal formalism, effective conductivities, and weak approximation, *Water Resour. Res.*, *29*(2), 341–364, doi:10.1029/92WR02062.

Nwankwor, G. I., J. A. Cherry, and R. W. Gillham (1984), A comparative study of specific yield determinations for a shallow sand aquifer, *Ground Water*, *22*, 764–772.

Nwankwor, G. I., R. W. Gillham, G. Vanderkamp, and F. F. Akindunni (1992), Unsaturated and saturated flow in response to pumping of an unconfined aquifer—Field evidence of delayed drainage, *Ground Water*, *30*(5), 690–700.

Oliver, D. S. (1993), The influence of nonuniform transmissivity and storativity on drawdown, *Water Resour. Res.*, *29*(1), 169–178, doi:10.1029/92WR02061.

Russo, D. (1988), Determining soil hydraulic properties by parameter estimation: On the selection of a model for the hydraulic properties, *Water Resour. Res.*, *24*(3), 453–459, doi:10.1029/WR024i003p00453.

Sánchez-Vila, X., J. P. Girardi, and J. Carrera (1995), A synthesis of approaches to upscaling of hydraulic conductivities, *Water Resour. Res.*, *31*(4), 867–882, doi:10.1029/94WR02754.

Srivastava, R., and T.-C. J. Yeh (1992), a three dimensional numerical model for water flow and transport, *Adv. Water Res.*, *15*, 275–287.

Straface, S., T.-C. J. Yeh, J. Zhu, S. Troisi, and C.-H. Lee (2007), Sequential aquifer tests at a well field, Montalto Uffugo Scalo, Italy, *Water Resour. Res.*, *43*(7), W07432, doi:10.1029/2006WR005287.

Streltsova, T. D. (1988), *Well testing in heterogeneous formations*, Wiley, New York.

Tartakovsky, D. M., and S. P. Neuman (1998), Transient flow in bounded randomly heterogeneous domains: 1. Exact conditional moment equations and recursive approximations, *Water Resour. Res.*, *34*(1), 1–12, doi:10.1029/97WR02118.

Tartakovsky, G. D., and S. P. Neuman (2007), Three-dimensional saturated-unsaturated flow with axial symmetry to a partially penetrating well in a compressible unconfined aquifer, *Water Resour. Res.*, *43*(1), W01410, doi:10.1029/2006WR005153.

Tiedeman, C. R., P. A. Hsieh, and S. B. Christian (1995), Characterization of a high-transmissivity zone by well test analysis: Steady state case, *Water Resour. Res.*, *31*(1), 27–37, doi:10.1029/94WR01965.

Wen, J.-C., C.-M. Wu, T.-C. J. Yeh, and C.-M. Tseng (2010), Estimation of effective aquifer hydraulic properties from an aquifer test with multi-well observations (Taiwan), *Hydrogeol. J.*, *18*(5), 1143–1155, doi:10.1007/s10040-010-0577-1.

Wu, C.-M., T.-C. J. Yeh, J. Zhu, T.-H. Lee, N.-S. Hsu, C.-H. Chen, and A. F. Sancho (2005), Traditional analysis of aquifer tests: Comparing apples to oranges, *Water Resour. Res.*, *41*(9), W09402, doi:10.1029/2004WR003717.

Xiang, J., T.-C. J. Yeh, C.-H. Lee, K.-C. Hsu, and J.-C. Wen (2009), A simultaneous successive linear estimator and a guide for hydraulic tomography analysis, *Water Resour. Res.*, *45*(2), W02432, doi:10.1029/2008WR007180.

Yeh, T.-C. J., and S. Liu (2000), Hydraulic tomography: Development of a new aquifer test method, *Water Resour. Res.*, *36*(8), 2095–2105, doi:10.1029/2000WR900114.

Yeh, T.-C. J., and J. Zhang (1996), A geostatistical inverse method for variably saturated flow in the vadose zone, *Water Resour. Res.*, *32*(9), 2757–2766, doi:10.1029/96WR01497.

Yeh, T.-C. J., R. Srivastava, A. Guzman, and T. Harter (1993), A numerical model for water flow and chemical transport in variably saturated porous media, *Ground Water*, *31*(4), 634–644.

Yeh, T.-C. J., A. L. Gutjahr, and M. Jin (1995), An iterative cokriging-like technique for ground-water flow modeling, *Ground Water*, *33*(1), 33–41.

Yeh, T.-C. J., M. Jin, and S. Hanna (1996), An Iterative Stochastic Inverse Method: Conditional Effective Transmissivity and Hydraulic Head Fields, *Water Resour. Res.*, *32*(1), 85–92, doi:10.1029/95WR02869.

Zhang, J., and T.-C. J. Yeh (1997), An iterative geostatistical inverse method for steady flow in the vadose zone, *Water Resour. Res.*, *33*(1), 63–71, doi:10.1029/96WR02589.

Zhu, J., and T.-C. J. Yeh (2005), Characterization of aquifer heterogeneity using transient hydraulic tomography, *Water Resour. Res.*, *41*, W07028, doi:10.1029/2004WR003790.

Zhu, J., and T.-C. J. Yeh (2008), Hydraulic tomography to characterization of heterogeneity of unconfined aquifers, paper presented at AGU Fall Meeting, San Francisco, California.

Zhu, J., T.-C. J. Yeh, and D. Mao (2011), Hydraulic tomography to characterize heterogeneity of unconfined aquifers, *J. Nanjing Univ.*, *47*(3), 252–264.